Taimuri, Ghalib; Ruponen, Pekka; Hirdaris, Spyros

A novel method for the probabilistic assessment of ship grounding damages and their impact on damage stability

Published in:
STRUCTURAL SAFETY

DOI:
10.1016/j.strusafe.2022.102281

Published: 01/01/2023

Document Version
Publisher's PDF, also known as Version of record

Structural Safety 100 (2023) 102281

Contents lists available at ScienceDirect

Structural Safety

journal homepage: www.elsevier.com/locate/strusafe

A novel method for the probabilistic assessment of ship grounding damages and their impact on damage stability

Ghalib Taimuri [a], Pekka Ruponen [a,b], Spyros Hirdaris [a,*]

[a] Department of Mechanical Engineering, Marine Technology, Aalto University, 02150 Espoo, Finland
[b] NAPA, Helsinki, Finland

A R T I C L E I N F O

Keywords:
Probabilistic modelling
Fluid-structure Interactions
Accidental loads
Monte carlo simulation
Grounding dynamics
Ship damage stability

A B S T R A C T

Existing statistics for use in ship damage stability assessment are based on either accident investigation reports or empirical crew records. This is the reason why the databases used within the context of ship design for safety are either incomplete or miss critical information. This paper introduces a methodology for the probabilistic evaluation of passenger ship damage extents. The model accounts for the influence of crashworthiness in real operational conditions. Based on operational statistical records for ships before grounding, a Monte Carlo simulation is utilized to randomly generate a realistic profile that accounts for variable ship speed, conical rock geometry, rock position, and height in both deep and shallow waters. Subsequently, using the operational parameters as input, a six degrees of freedom fluid–structure interaction (FSI) model is used to combine the influence of ship dynamics, and structural mechanics on the probability distributions of hull breaches. Ship damage stability evaluation is carried out using NAPA software, which measures ship survivability via an attained subdivision index. Probabilistic results are compared against existing distributions of damage extents and demonstrate an increase in the mean distribution of damage length. The findings demonstrate the method's adequacy for improving passenger vessel safety in case of ship grounding. It is concluded that the method allows for low-fidelity optimization of the structural arrangement of the bottom of the ship, probabilistic evaluation of loads associated with ship crashworthiness, and the assessment of operational limitations during an evasive maneuver. It could therefore be used for the future development of ship damage stability standards or ad - hoc forensic investigations.

1. Introduction

Shipping propels 90 % of world trade. In recent years, the demands of the economies of scale lead to increased ship sizes, traffic complexity and inevitably accidents associated with extreme operational scenarios. Based on recent accident records critical factors associated with serious maritime accidents are collisions, fires, and hard groundings [1]. Amongst these unfortunate events, groundings are the most frequent yet the least understood events.

A grounding accident may occur when ships collide with a seabed obstruction. Regardless of the root causes, consequences with impact on property, environmental pollution and loss of human life can be detrimental [2]. This statement is well justified by the statistical accident records of the Helsinki Commission (HELCOM), according to which between 2000 and 2018 776 occurrences took place in the Baltic Sea area [3] (see Fig. 1). Notably, these statistics confirm that passenger vessels are the second most vulnerable to ship grounding accidents after cargo ships.

A critical review of the recent groundings of Akademik Ioffe in 2018 (attributed to incomplete information on bathymetry) [4], Amorella in 2020 (attributed to propulsion system malfunctioned) [5], Viking Grace in 2020 (attributed to stormy and gusty winds) [6], demonstrates that good operational practice is essential under uncertain environmental conditions; otherwise, ship flooding and loss of damage stability may

* Corresponding author.
E-mail address: spyros.hirdaris@aalto.fi (S. Hirdaris).

https://doi.org/10.1016/j.strusafe.2022.102281
Received 19 March 2022; Received in revised form 5 September 2022; Accepted 6 September 2022
Available online 22 September 2022

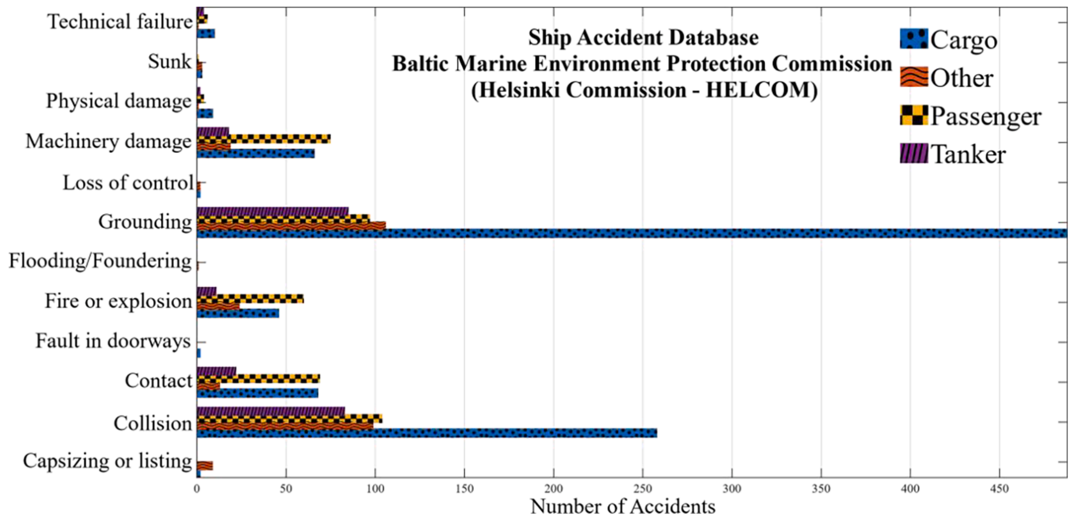

Fig. 1. Accident statistics in the Baltic Sea from 2000 to 2018, data from [3].

lead to environmental pollution and loss of life. It is therefore important to establish tools and methods that can evaluate how long a ship can stay afloat in real operational conditions (e.g., see accident investigation reports for Monarch of the Seas [7], Express Samina [8] and Costa Concordia [9] accidents).

Understanding the dynamics of ship grounding from an operational perspective requires a sound combination of ship science and design practice. In this sense, the combination of principles of ship strength (loads and responses in real environmental conditions) and damage stability within the context of probabilistic mechanics should be considered practical and impactful from a ship safety perspective.

To date, ship crashworthiness during grounding events has been analyzed using finite element analysis (FEA) or empirical methods [10]. For example, existing models for the evaluation of penetration damages following grounding events have been investigated in terms of material fracture and plastic deformation [10,11]. In literature, several authors utilized experiments and FEA tools to develop mathematical equations expressing the resistance forces of hull bottom structures [12,13,14,15,16]. Accordingly, empirical equations have been developed for the simple calculation of structural reaction forces during impact. In these methods, the structural resistance of individual parts of the hull (plates, stiffeners, bulkheads, girders, and floors) is evaluated and their aggregate is used to assess the hull bottom deformation at the time of the accident [17,18,19,20,21,22].

Large scale multiphysics crashworthiness methods can provide useful advancements in terms of exploring the influence of fluid actions on grounding dynamics [23,24,25,26]. These methods combine non-linear FEA with potential flow hydrodynamics while accounting for ship operations, and seabed evasion. Recent research demonstrates that practical limitations associated with the computational economy of these large scale methods may be overtaken by the use of the super-element technique [27] or simplistic contact mechanics models [28]. Yet, the broader appreciation of uncertainties associated with environmental conditions (such as shallow water, short waves, wind, and ocean currents), ship particulars (operating draft), operating conditions (velocity, bathymetry, seabed profile, human decision), ship's maneuverability and their influence on ship safety remain under development [29,30].

Probabilistic damage mechanics could suggest a feasible framework for the evaluation of stochastic ship grounding dynamics and associated effects on damage stability. Furthermore, ship grounding hazard is linked with risk and sustainability, where environmental, social, and economic metrics of ship grounding can be assessed by using the probabilistic damage mechanics of the ship [31]. The basis of a potentially promising probabilistic assessment approach for the assessment of ship survivability following grounding events is proposed in [32]. In this so-called non-zonal analysis method, the damage distribution of passenger and container ships grounding is based on existing accident investigation reports [33,34]. Monte Carlo simulations are used to idealise the influence of a box-shaped ship damage geometry on ship damage stability following ship collisions [35,36]. The method can be used within the context of International Maritime Organization (IMO) probabilistic damage regulations for ship collisions. However, it does not account for structural arrangements and variations in operational conditions (traffic or environmental) or ship dynamics. A recent study also shows the benefit of using sampling methods apart from Monte Carlo simulations (such as the Latin Hypercube and Randomized Quasi-Monte Carlo) to minimize sampling sizes with the least variability in estimating ship survivability [37].

Recently, Zhang et al. [38] proposed a direct assessment method that utilizes automatic identification system AIS data in combination with a structural deformation model [39] for the assessment of ship damage stability following collision events. This approach opens a new direction for rapid crashworthiness assessment and the deterministic definition of collision damages for ad-hoc operational scenarios. Notwithstanding this, understanding the influence of ship grounding dynamics and their impact on damage stability remains unknown. This is because most grounding contact avoidance methods do not consider the influence of external ship dynamics. Instead, they are based on the probabilistic approach of the geometric distribution of the ship traffic profile [40] or damage distributions generated from sparsely populated historical data records [35]. By analyzing AIS information, precise traffic distribution data can be obtained for a region. However, even this approach does not take into account the maneuverability of the vessel [29]. Additionally, prior research indicates that damage distributions based on historical damage data do not incorporate ship structural design or accident scenarios. [32,35,41,42]. This limits the effect of real-world traffic scenarios and environmental conditions [27].

This paper makes use of the rapid FSI model of Taimuri et al. [28] to estimate probabilistic damage extents following the grounding of a passenger ship in real environmental conditions. The method utilizes Monte Carlo simulations to generate the ship operating parameters, the conical rock profile [43], which is then used as an input to 6-DoF maneuvering [44,45] and a structural deformation model [17,21,28]. The method helps determine the extents of damage, the maximum resistance force to the structure, and the maximum achievable rupture path of the ship during grounding. The probability distributions of the damage extents developed by a novel method are transferred into the NAPA[1] software to assess ship survivability [46]. The focus of the paper is to explore the "actual damage" in way of a ship's bottom while accounting for the size of the rock and ship maneuverability in real conditions. The ultimate goal is to populate a probabilistic database for use in ship damage stability analysis or structural crashworthiness assessment following hard grounding events.

This paper makes use of a NAPA 3D passenger ship model namely FLOODSTAND Ship B presented by [47]. This 3D ship model includes a buoyant hull and all compartments inside the hull, namely tanks, machinery rooms, crew accommodation, stores, etc. The NAPA damage stability solver is designed to analyze vessel survivability if one or more of these compartments are damaged and/or flooded. Following the modelling of the damage extents, the software calculates the righting lever curve for each flooding stage of the damage and evaluates the s-factor as per SOLAS2020 Chapter II-1 Part B-1 Regulation 7-2. The p-factor and attained index are obtained as discussed in section 4.

The grounding solver is a rapid grounding dynamics model, which combines 6-DoF ship maneuvering motions with a model accounting for structural deformations and the influence of hydrodynamic properties in way of grounding contact [28]. The model advances the state of the art by allowing for.

1) Implementation of varying plate split angles (where the plate split angle represents the extent of plate deformation ahead of the conical rock);
2) Variation of the inner and outer bottom plate split angles that were considered equivalent in past models [17,21];
3) Evaluation of dynamic rock–ship interactions, through a rapid coupling algorithm that combines internal and external mechanics at the interface of the rock tip with the ship's bottom.

Earlier grounding assessment models, such as the grounding and collision analysis toolkit GRACAT [48], did not include the attributes listed above. Furthermore, the model by Taimuri et al. [28] has been tested against non-linear FEA simulations using the commercial solver LSDYNA-MCOL. To investigate ship grounding, a commercial coupled nonlinear FEA FSI model may be used to provide more accurate results. However, the primary limitation of adopting these FEM and FSI models is the high computational cost, which makes them non-feasible within the context of rapid crashworthiness assessment and probabilistic analysis.

Section 2 of the paper presents an overview of the method. Section 3 provides an overview of the rapid 6-DoF FSI solver, which includes a summary of external mechanics, internal mechanics, and the contact coupling algorithm. Section 4, briefly outlines the procedure of ship survivability after flooding. In section 5, the methodology used for the damage profile modelling governed by the FSI solver is explained in detail. Section 6, discusses the result of the simulations, compares damage with historical data, and provides a realistic probability density function of damage extents, maximum forces, and ship motions. Conclusions are presented in section 7.

2. Methodology

The methodology is depicted in Fig. 2 and comprises the following building blocks:

- At first, the probabilities of the ship operation and environmental condition before the accidents described in the statistics of Youssef and Paik are considered [43]. These statistical distributions include information on the velocity of the ship before grounding, the eccentricity of the rock with respect to the ship centerline and rock height / tip radius / semi-apex angle. Bathymetry is obtained from HELCOM [3] accident statistics.
- The probability distributions are embedded into the two-way coupled 6-DoF rapid multiphysics solver. A series of Monte Carlo simulations that consider the influence of FSI and conical rock geometry are carried out. At each step of the simulations, the location of the rock is searched. For those cases where the rock gets in contact with the hull,the damage penetration, width, and length are evaluated. The contact algorithm accounts for structural deformations and ship motions in all 6-DoF. The probabilities of the damage extent, maximum ship motions, structural resistance forces, and deformation energy are generated.
- The resultant damage extents are transferred into NAPA software to estimate the probability of flooding of a single compartment or compartment groups (*p*-factor).
- Based on the damaged compartment(s), the survivability factor (*s*-factor) is calculated as defined in the safety of life at sea SOLAS2020 Chapter II-1 Part B-1 Regulation 7–2. These are in line with the procedure followed by Bulian et al. [32,35], for damage ship survivability assessment.

3. Summary of the grounding dynamics solver used to assess the ship's damage

The grounding dynamics solver used to assess the ship's damage is described by Taimuri et al. [44,28]. The governing mathematical formulation of this model is given in Equation (1).

$$
\begin{aligned}
&Surge\ E.O.M: \left(m - X_{\dot u}\right)\dot u + \left(mz_G - 0.5\ X_{\dot u}T\right)\dot q \\
&\quad = m\left(rv + x_G\left(r^2 + q^2\right) - wq - z_G pr\right) + \rho g A_{WP}(\Delta z)\sin(\theta) + X_{Hull} \\
&+ X_{Res}(1-t) + X_{Prop} + X_{Rud} + X_{Wind} + X_{Waves_{Short}} + X_{C,GRD} \qquad (1)\\[6pt]
&SwayE.O.M: \left(m - Y_{\dot v}\right)\dot v - \left(mz_G + Y_{\dot p}\right)\dot p + \left(mx_G - Y_{\dot r}\right)\dot r \\
&\quad = m(pw - ru - z_G qr - x_G pq) - \rho g A_{WP}(\Delta z)\sin(\phi)\cos(\theta) \\
&+ Y_{Hull} + Y_{Rud} + Y_{wind} + Y_{Waves_{Short}} + Y_{C,GRD}\\[6pt]
&HeaveE.O.M: \left(m - Z_{\dot w}\right)\dot w - \left(mx_G + Z_{\dot q}\right)\dot q \\
&\quad = m\left(uq - vp + z_G\left(p^2 + q^2\right) - x_G rp\right) - \rho g A_{WP}(\Delta z)\cos(\phi)\cos(\theta) \\
&- 2\zeta_w \omega_w w\left(m - Z_{\dot w}\right) + Z_{C,GRD}\\[6pt]
&RollE.O.M: -\left(mz_G + K_{\dot v}\right)\dot v + \left(I_X - K_{\dot p}\right)\dot p - \left(mx_G z_G + K_{\dot r}\right)\dot r \\
&\quad = m(z_G ur - z_G wp + x_G z_G pq) + (I_Y - I_Z)qr \\
&\quad - \rho g \nabla GM_T \sin(\phi)\cos(\phi)\cos(\theta) + K_{Hull} + K_{Rud} + K_{Wind} + K_{Waves_{Short}} \\
&- 2\zeta_\phi \omega_\phi p\left(I_X - K_{\dot p}\right) + y_{int} Z_{C,GRD} - z_{int} Y_{C,GRD}\\[6pt]
&PitchE.O.M: \left(mz_G - 0.5X_{\dot u}T\right)\dot u - \left(mx_G + Z_{\dot q}\right)\dot w + \left(I_Y - M_{\dot q}\right)\dot q \\
&\quad = m\left(z_G vr - z_G wq + x_G vp - x_G uq - x_G z_g\left(p^2 - r^2\right)\right) + (I_Z - I_X)pr - \rho g \nabla GM_L \sin(\theta)\cos(\phi)\cos(\theta) \\
&+ M_{Rud} - 2\zeta_\theta \omega_\theta q\left(I_Y - M_{\dot q}\right) - x_{int} Z_{C,GRD} + z_{int} X_{C,GRD}\\[6pt]
&YawE.O.M: \left(mx_G - N_{\dot v}\right)\dot v - \left(mx_G z_G + K_{\dot r}\right)\dot p + \left(I_Z - N_{\dot r}\right)\dot r \\
&\quad = m(x_G wp - x_G ur - x_G z_G qr) + (I_X - I_Y)pq \\
&\quad - \rho g \nabla\left(-GM_L\cos(\theta) + GM_T\right)\sin(\phi)\sin(\theta) + N_{Hull} + N_{Rud} + N_{Wind} \\
&+ N_{wave_{Short}} + x_{int} Y_{C,GRD} - y_{int} X_{C,GRD}
\end{aligned}
$$

[1] NAPA [67] is a commercial software package for marine engineering design. The software includes sophisticated hydrodynamics, seakeeping, hydrostatics, damage stability solvers. It also allows for 3D geometry modelling of the hull surface and compartments. These are just a few attributes of NAPA software. Detailed descriptions and examples of application of the program are found in [67].

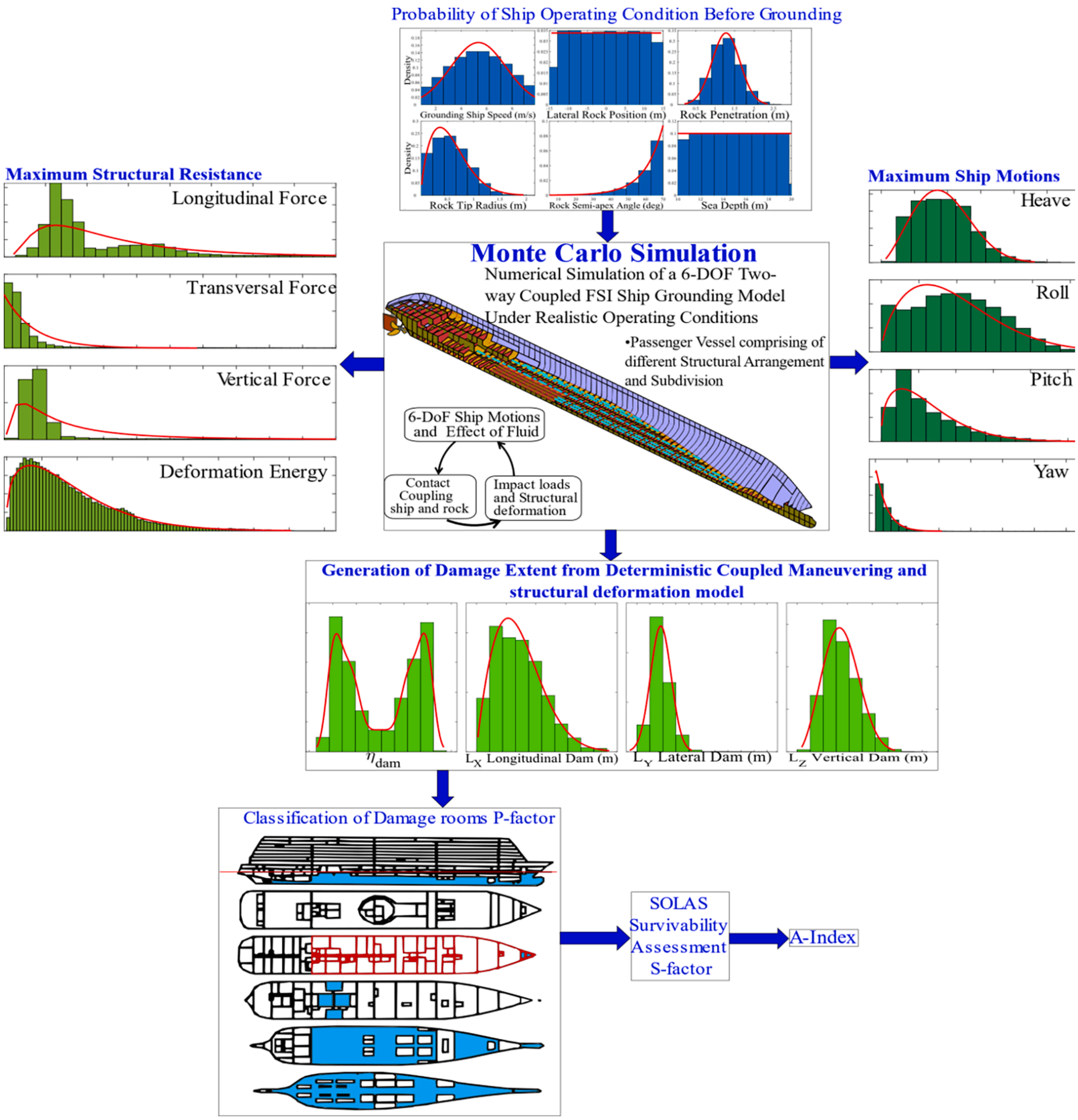

Fig. 2. A rapid FSI methodology for the probabilistic assessment of the extents of damage, structural deformation, and maximum ship motions following a grounding event.

In the above equation $\dot{u}, \dot{v}, \dot{w}, \dot{p}, \dot{q},$ *and* $\dot{r}$, represent surge, sway, heave, roll, pitch and yaw acceleration respectively. The acceleration subscripts terms $(X_{\dot{u}}, Y_{\dot{v}}, Y_{\dot{p}}, Y_{\dot{r}}, Z_{\dot{w}}, Z_{\dot{q}}, K_{\dot{v}}, K_{\dot{p}}, K_{\dot{r}}, M_{\dot{q}}, N_{\dot{v}}, N_{\dot{r}})$ represent the hydrodynamic added masses and added inertia forces that arise from the deflection of the surrounding fluid. The mass 'm' multiplier components on the right-hand side indicate the Coriolis and centripetal forces caused by the rotation of the body-fixed coordinate system about the inertial frame. The translation velocities in the surge, sway and heave directions are u, v *and* w, respectively; $p, q,$ *and* r, represent roll, pitch and yaw motions respectively. The density 'ρ' and gravity 'g' multiplier terms are restoring forces, that depend on waterplane area A_{wp}, the instantaneous change in heave displacement Δz and angular roll ϕ and pitch θ rotations of the ship. Additionally, the restoring moments depend on transverse GM_T and longitudinal GM_L metacentric height. The contact forces at the location of the rock $(x_{int}, y_{int},$ *and* $z_{int})$ ship interface are $X_{C,GRD}$, $Y_{C,GRD}$ *and* $Z_{C,GRD}$. Hydrodynamic damping forces are denoted by the subscript namely "*Hull*". The remaining terms describe control forces ("*prop*", "*Rud*"), environmental forces ('$wave_{Short}$', '*Wind*'), and ship resistance ('*Res*') and are discussed in subsequent sections.

3.1. Ship maneuvering dynamics

The maneuvering model assumes calm water resistance X_{Res} for the case of a ship moving at a straight course. This can be obtained either from statistical regression [49] or from Model tests or computational fluid dynamic CFD solvers. Ship propulsion X_{Prop} and rudder forces (subscript '*Rud*' Equation (1)) are defined in [50,51,44]. Aerodynamics play an influential role in ship dynamics, where the loads are dependent on time and location due to the stochastic nature of the wind. The evaluation of wind loads on a ship (subscript '*Wind*' Equation (1)) is given in [51,52], where the coefficients of wind forces are estimated according to Blendermann [53]. This study does not demonstrate the influence of wind loads on grounding dynamics. However, for the completeness of the method wind loads are idealised as reported in [52].

The model accounts for short waves (wavelength to ship length ratio of $\lambda/Lpp \leq 0.5$), heading and speed before the grounding impact. Hydrodynamic resistance in short waves is based on the models of Sakamoto and Baba [54], and Faltinsen [55,56]. The hull forces acting on the ship during maneuvering are expressed by hydrodynamic derivatives. These forces acting on the ship hull account for ship velocity and acceleration and are presented in [44]. The radiation damping associated with heave, roll, and pitch motions (see ζ multiplier terms in Equation (1)) is considered linear and depends on the natural period of the ship under small amplitude motions. A description of the reference technique that accounts for the change in the hydrodynamic assumption of hull forces for a twin-screw vessel is given in [27]. In a typical grounding scenarios, the effect of shallow waters on ship resistance may be significant [52]. Accordingly, the viscous resistance corrections proposed by Raven have been implemented in the model [57]. The influence of shallow water effects on hydrodynamic coefficients is implemented as per Ankudinov et al. [58] and Kijima et al. [59]. Fig. 3 illustrates the numerical integration method used to evaluate the ship trajectories and

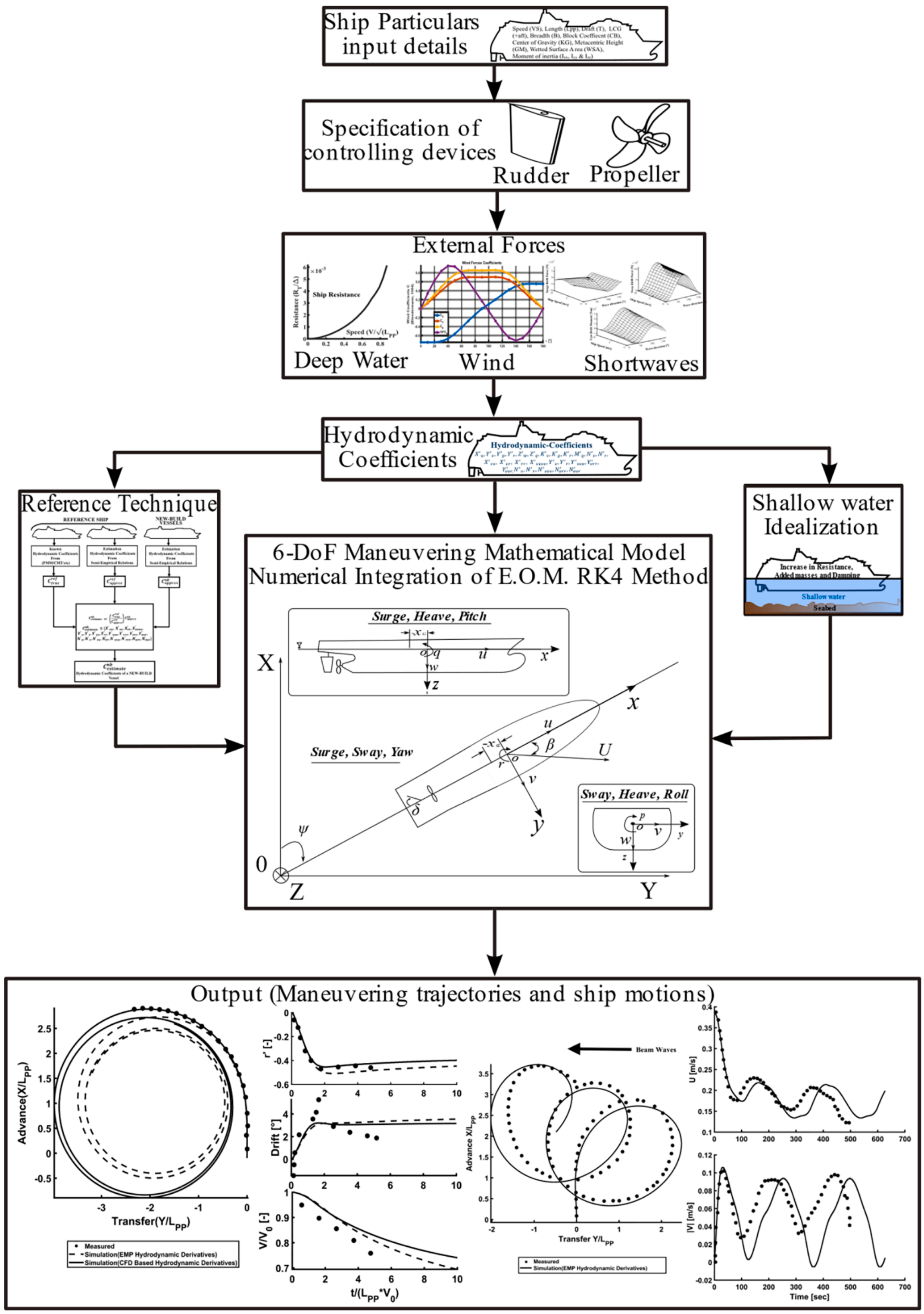

Fig. 3. Flow chart and modelling approach of ship external dynamics analysis.

motions. The external dynamics are presented and validated in Taimuri et al. [44].

3.2. Bottom structural deformation

The contact forces and moments (subscript 'C, GRD', Equation (1)) originated from the impact between the ship bottom and rock. The detailed formulation for the evaluation of accidental loads following ship hard grounding can be found in Taimuri et al. [28]. The loads from contact with the rock were realized based on the so-called "energy-based criteria of deformable bodies", i.e., the rock was assumed rigid, the structure is considered to be rigid-plastic and the effect of elastic energy is ignored in the resulting deformation following contact. This method accounts for bottom structural deformations presented by Simonsen [17] and Sun et al. [21]. Accordingly, the energy dissipation is obtained from the integration of the stress and strain fields over the volume of the structure and the upper-bound method of plasticity given in Equation (2) [17].

$$\boldsymbol{F_H U} = \dot{\boldsymbol{E}}_p + \dot{\boldsymbol{E}}_c + \dot{\boldsymbol{E}}_f = \boldsymbol{F_P.U} + \int_S \boldsymbol{p\mu U_{rel} dS} \tag{2}$$

In the above expression, F_H is the resisting force of the structure in the direction of U; U is the relative velocity between the ship and a rock; $\dot{E}_p, \dot{E}_c, \dot{E}_f$ express the rate of plastic, crack, and frictional energy dissipation respectively; F_P is the plastic resistance which includes both plasticity and fracture; μ is the Coulomb coefficient of friction; p is the normal pressure on the rock from the plate element dS; S is the contact area between rock and plate; U_{rel} is the relative velocity between rock and plate element dS.

Grounding over a rigid object is idealized by a conical rock with a rounded tip of radius R_R and semi-apex angle ϕ. The structural components depicted in Fig. 4 consist of the inner and outer shell of the hull, longitudinal girders, bulkheads, stiffeners, and transverse floors. Forces generated by individual structural components are resultant contact forces at a particular position along the grounding path. The hull outer bottom holds the structural components (floors, girders, bulkheads, and stiffeners) which are attached to the shell plate. Therefore, the global mode of deformation is governed by the outer hull plating.

Depending on the deformation mode of the ship's bottom structure the vessel may experience stretching, bending and/or fracture [28]. The outer bottom of the hull while in contact with the rock, may tear the plate with a split angle θ (Fig. 4). Practically, θ represents the extent of the plate deformation ahead of the conical rock. Taimuri et al. [28], highlight the importance of properly evaluating the plate split angle by demonstrating a comparison of values obtained from the FEM solver against the theoretically minimized resistance force approach introduced by Simonsen [17]. It is confirmed that the implementation of varying plate tearing angles provides more realistic predictions of horizontal and vertical forces.

3.3. Fast contact detection algorithm for ship panel and rock

A fast contact detection algorithm has been developed to locate the interface between the ship panel hull and the tip of a conical rock [28]. The contact between the rock tip and hull panels activates the mechanism responsible for the movement of the ship and structural deformation due to impact loads. The outcome of the contact is hull penetration. Fig. 5a, illustrates the steps followed to locate the interface between the rock and hull panels. The coordinates of each triangular hull panel are defined in relation to the origin of the ship. These points are stored for the estimation of the contact search algorithm that operates as follows:

a) A grid is generated based on the main dimension of the hull and the number of blocks.
b) Panel IDs are stored in a specific block. The initialization steps point a) and b) occur only once.
c) The tip is defined as a point. From this point, a vector is assumed which is directed vertically towards the ship base (or seabed), Fig. 5b.
d) The relative distance between the ship origin and tip location helps identify the sub-block containing the rock.
e) The intersection between the tip vector and the hull panel is obtained using a Ray tracing algorithm [60,61].
f) Once the intersection is detected and based on the rock tip position and ship motions, the relative displacement is evaluated.

The displacement outputs from the contact search algorithm are utilized to estimate the structural deformation forces. Those are subsequently employed as an external force in the 6-DoF equation of motion (see Eq. (1)). Further details on the method can be found in [28].

4. Ship survivability following flooding condition

The method follows a non-zonal approach for damage stability assessment. Following damage, the survivability of a vessel is represented by an attained subdivision index 'A'. According to SOLAS2020 [62], for a ship to survive in a flooding condition attained index A should be larger than or equal to the required index R which depends on number of people on board. The formulation of the attained subdivision index for grounding damages A_{GR} used in the present model is given in Equation (3). This complies to the probabilistic damage stability criterion for ship survivability [32,35], expressed as:

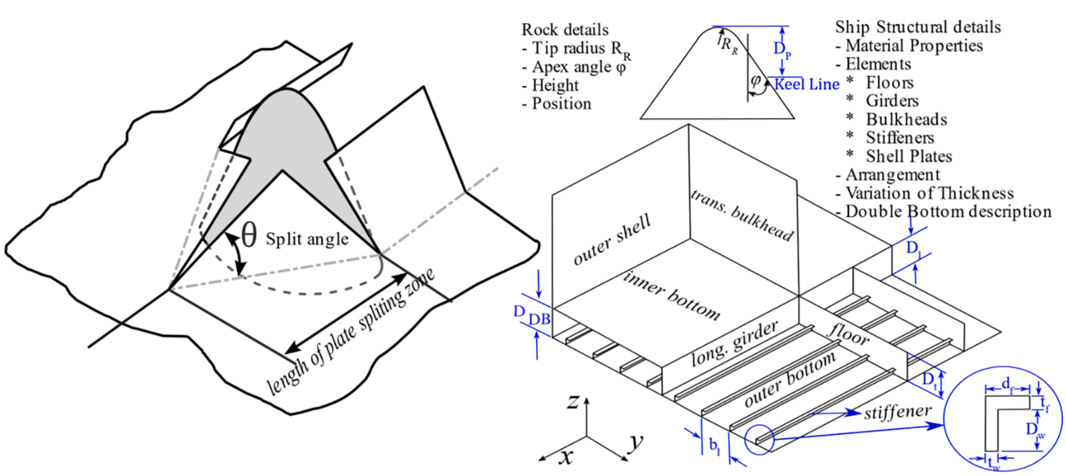

Fig. 4. idealization of ship bottom structural particulars, conical rock details and definition of plate splitting angle.

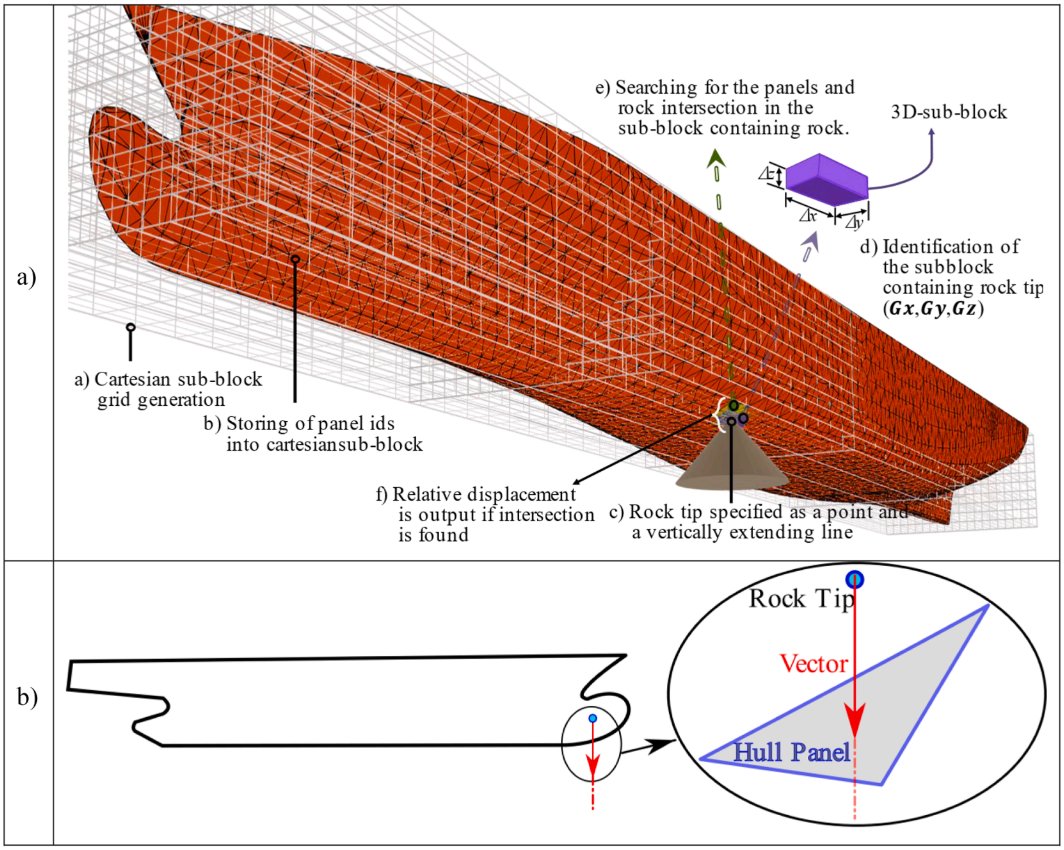

Fig. 5. Representation of the ship, rock, cartesian domain, intersection between the rock and panel, and the steps followed for rapid detection of contact.

$$A_{GR} = \sum_i p_i . s_i \tag{3}$$

where, i represents the cases of a compartment or a group of compartments that are damaged; p_i is the associated probability that the compartments are damaged (p-factor) and s_i represents the safety degree (s-factor) after flooding.

The IMO SOLAS 2020 regulations require three different drafts to acquire the attained subdivision index. As this paper focuses on demonstrating the FSI method instead of its broader impact on regulatory development only one design draft is considered. The *s-factor* is calculated according to SOLAS 2020 Chapter II-1 Part B-1 Regulation 7-2. The *p-factor* is defined as.

$$p_i = \frac{n_i}{N_T} \tag{4}$$

where, n_i shows the damage cases having the same groups of compartments being breached and N_T is the total number of performed simulations.

A Monte Carlo simulation is performed to generate the hull breaches (damage extents) by utilizing the deterministic FSI ship grounding dynamics solver described in Section 3. These damage statistics are transferred into the NAPA software, which can model the damaged rooms for each breach case and calculate A_{GR}. The details of the modelling assumptions and the procedure for the evaluation of the p- and s-factors can be found in [63,64,46].

5. Damage characteristics and input parameters

5.1. Ship damage profile following grounding

The deterministic damage profile computed from the rapid FSI method accounts for the maximum coordinates of the damage extents. The numerical assessment of ship grounding over a conical rock provides detailed deformation characteristics elaborated in Figs. 6-8. The location of the damage coordinates follows a right-handed coordinate system with the origin attached in way of the centerline and ship aft perpendiculars.

The first contact between the rock and hull bottom is denoted as X_F. This is the point that governs the length of the damage, and transversal (starboard and portside) limits of the hull bottom $b(X_F, z^*)$ depicted in Fig. 6. The vertical position of the first contact from the keel line is

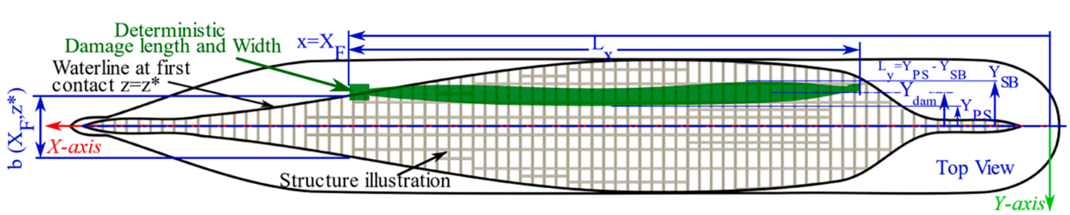

Fig. 6. illustration of deterministic longitudinal and transverse damage extent of a ship. Top view XY plane. The x-axis points toward the bow (positive), the y-axis is positive towards the portside.

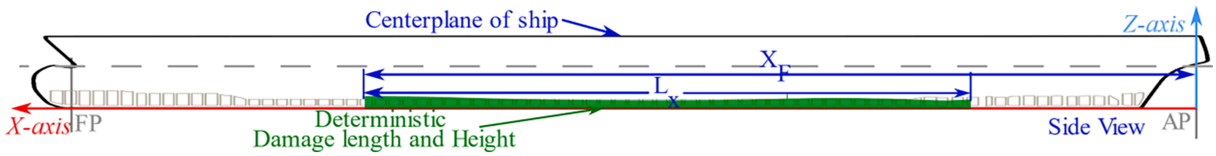

Fig. 7. illustration of deterministic longitudinal and vertical damage extent of a ship. Side view XZ plane. The z-axis is positive upward from the base keel line.

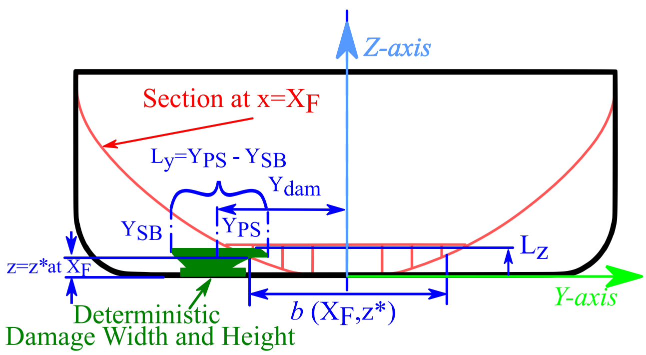

Fig. 8. illustration of deterministic transverse and vertical damage extents of a ship. Front view YZ plane.

defined as z^*. The total length of the damage is L_x as shown in Fig. 7. The transversal extent of the damage width namely L_y is formed by the extreme extent of the damage towards starboard - side (Y_{SB}) and port-side (Y_{PS}). The center of measured damage (Y_{dam}), shows the distance from ship centerline ($y = 0$) to the midpoint of the transverse damage (see Fig. 6,8). The center of measured damage is included in the damage profile using the following equation:

$$\eta_{dam} = Y_{dam}/b(X_F, z^*) \tag{5}$$

where, η_{dam} represents the non-dimensional center of measured damage with respect to the transverse limit of the hull at the very first contact. By utilizing the limits of the damage coordinates throughout the deterministic grounding simulation, a box shape damage profile is formed (see Fig. 9). This is then used for the evaluation of p- and s-factors.

Well-established probabilistic approaches for the assessment of damaged ship structures, build their models on the basis of historical records [36,35,32]. These damage distributions are based on statistical analysis of available data from past accidents. In these distributions the grounding data of passenger and container ships accounting for available accident records were combined [36]. The addition of container ships was considered useful attribute especially considering that grounding accidents involving passenger ships are very few.

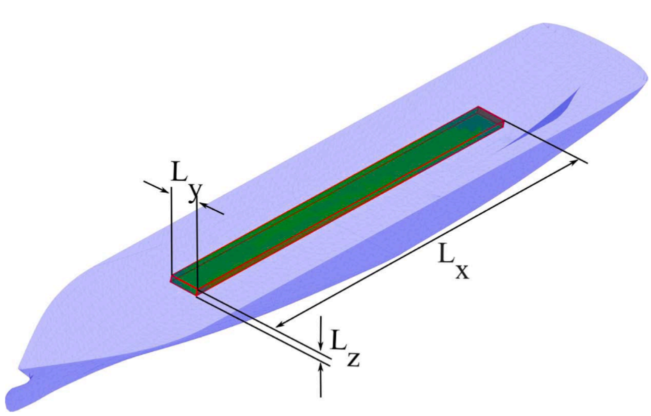

Fig. 9. illustration of box shape damage formation from the deterministic damage profile.

Additionally, existing damage distributions do not account for detailed conditions of the ship structure, environmental conditions, and the influence of the surrounding environment. The probabilistic ship accident modelling based on historical data do not account for the influence of traffic conditions and associated navigational variables [2].

The historical probability density function simply provides the ship's (longitudinal, transversal, and vertical) damage extent which depends on the design length, breadth, and draft of the ship. These models assume the *"potential damage"* that may extend beyond the vessel's limit partially extending from either port - or starboard - side. These methods tend to overestimate the vertical and longitudinal extent of the damage. The fundamental advantage of damage profile modelling, as presented here, is that it is based on actual damage, which is not only formed within the ship domain, but is also affected by the structural details, ship motions, environmental force, and maneuvering conditions. The documentation of this "potential damage" distribution can be found in the EMSA-III report [36].

During a grounding simulation, the ship will translate and rotate because of the influence of rock dynamics (forces) leading to structural deformation. Ship heave, roll and pitch motions may lead to varying penetrations along her length. Ship yaw, sway and roll will deform the structure transversely; and the combined 6-DoF motion during grounding will contribute to the total longitudinal damage length. Notably, all these damage distributions are associated with environmental (deep and shallow waters) and operational (velocity, bathymetry and seabed profile) conditions.

5.2. *Probabilistic distributions for a passenger ship before grounding*

Simulations were based on the modern passenger vessel FLOODSTAND SHIP B [47] with structural details and principal particulars shown in Fig. 10. The subdivision of the vessel as shown in Fig. 11, illustrates the escape routes, unprotected openings, watertight compartments and cross-flooding pipes for the calculation of the s-factor. The validation of ship external dynamics (maneuvering) and internal mechanics (structural deformation) is presented in Taimuri et al. [28,44]. For the probabilistic assessment of the grounding of the ship, credible operating conditions are required to classify the grounding scenarios.

The operational and environmental factors that may contribute to a typical hard grounding scenario are modelled by random variables using the probability density function (pdf) of Youssef and Paik [43]. This model includes probability distributions of ship speed, trim angle, rock location with respect to ship centerline and rock profile for different types of vessels. Grounding characteristics (i.e., pdf of ship velocity, rock height, rock profile, rock eccentricity) were investigated for the following four conditions:

i) *passenger vessel* operational conditions, maneuvered in *deep waters*
ii) *passenger vessel* operational conditions, maneuvered in *shallow waters*
iii) *All-types of vessels* operating conditions, maneuvered in *deep waters*
iv) *All-types of vessels* operating conditions, maneuvered in *shallow waters*

The water is considered deep for sea depth to ship draft H/T ratio

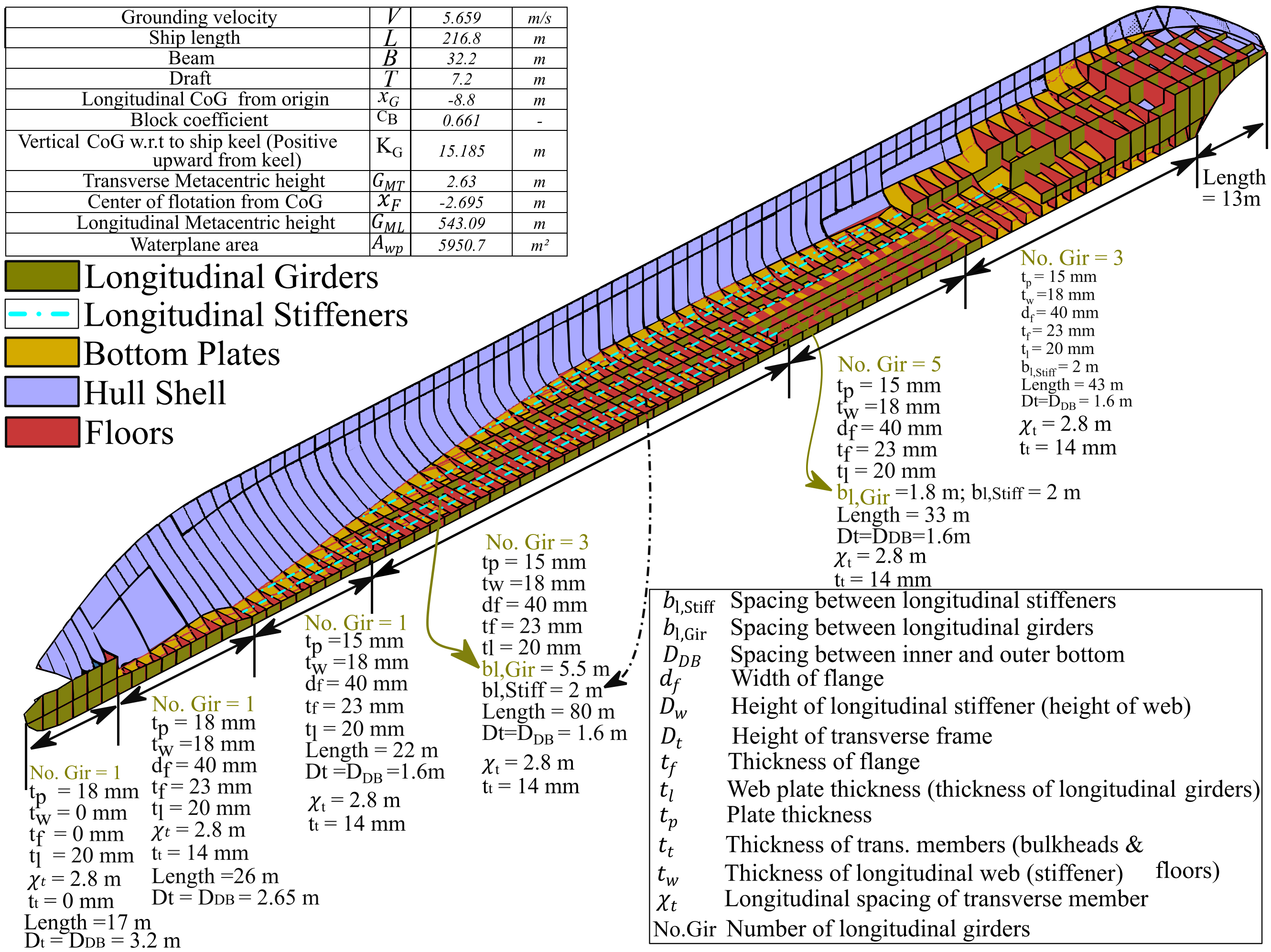

Fig. 10. Description of the structural arrangements, layout, dimensions and ship parameters of the FLOODSTAND SHIP B.

that is greater than 100. Shallow water was assumed to be equally distributed in the range $1.35 \le H/T \le 2.78$. Shallow water statistics were derived from maritime accidents in the Baltic Sea between 1989 and 2018 [3]. Table 1, presents a summary of statistics for the operating probability distributions of *passenger vessels* and *All-types of vessels*. This includes input pdf of rock eccentricity Y_{GR}, ship impact velocity V_i, rock depth D_p (which is the initial height of the rock-tip from keel line), rounded tip radius of rock R_R, and cone semi apex angle ϕ. The position of the rock tip was modelled as a uniform distribution with the bounds $X \in [-B/2, B/2]$, where the ship's centerline is considered zero.

The rock model by Youssef and Paik [43] is a paraboloid. The rock is formed from the damaged database of the EU GOALDS project [34]. Accordingly, the length, width and depth of the damage extents were utilized to create paraboloid rock parameters distribution. Contrary to this, in the present method, a conical rock is considered with a rounded tip radius and semi-apex angle. Therefore, it was assumed that the radius of the tip is 12.5 % of the width of the rock. The semi-apex angle was formed by averaging the width and length (of the paraboloid rock) as follows:

$$\phi = \tan^{-1}\left(\frac{l+w}{4d}\right) \tag{6}$$

In the above equation l, w *and* d are the distribution of length, width and depth of the rock as per Youssef and Paik [43].

6. Results and discussion

6.1. Probability distributions of grounding scenarios

Monte Carlo simulations were used to evaluate the degree of the damage, structural failure forces, and ship motions. A pseudorandom number generator based on Mersenne Twister [65] was implemented to produce input conditions based on the probability distributions indicated in Table 1. To account for uncertainties in input conditions (forces, motions, and A-index) a set of five repetitions with 20,000 simulations (5-different starting seeds and 4 conditions defined in Section 5.2) were considered. This is consistent with a recent analysis by EMSA [36], which recommends running 10,000 scenarios with five distinct seeds to achieve a reasonably adequate confidence interval for damage breaches.

Histograms of the randomly generated samples from the given input probability distributions displayed in Table 1 are shown in Fig. 12. Input factors were impact velocity, rock eccentricity, penetration depth, rock tip radius, apex angle, and sea depth to ship draft ratio for *All-types of vessels* and the *passenger vessel*. The sample means of the input distribution with 95 % confidence interval is shown in Fig. 13. An important observation from the statistical analysis [43] is that the mean value of penetration depth and rock tip radius encountered by *passenger vessel* is greater than the statistics for *All-types of vessels*, where the mean value of penetration depth and tip radius is 80 % and 45 % higher respectively.

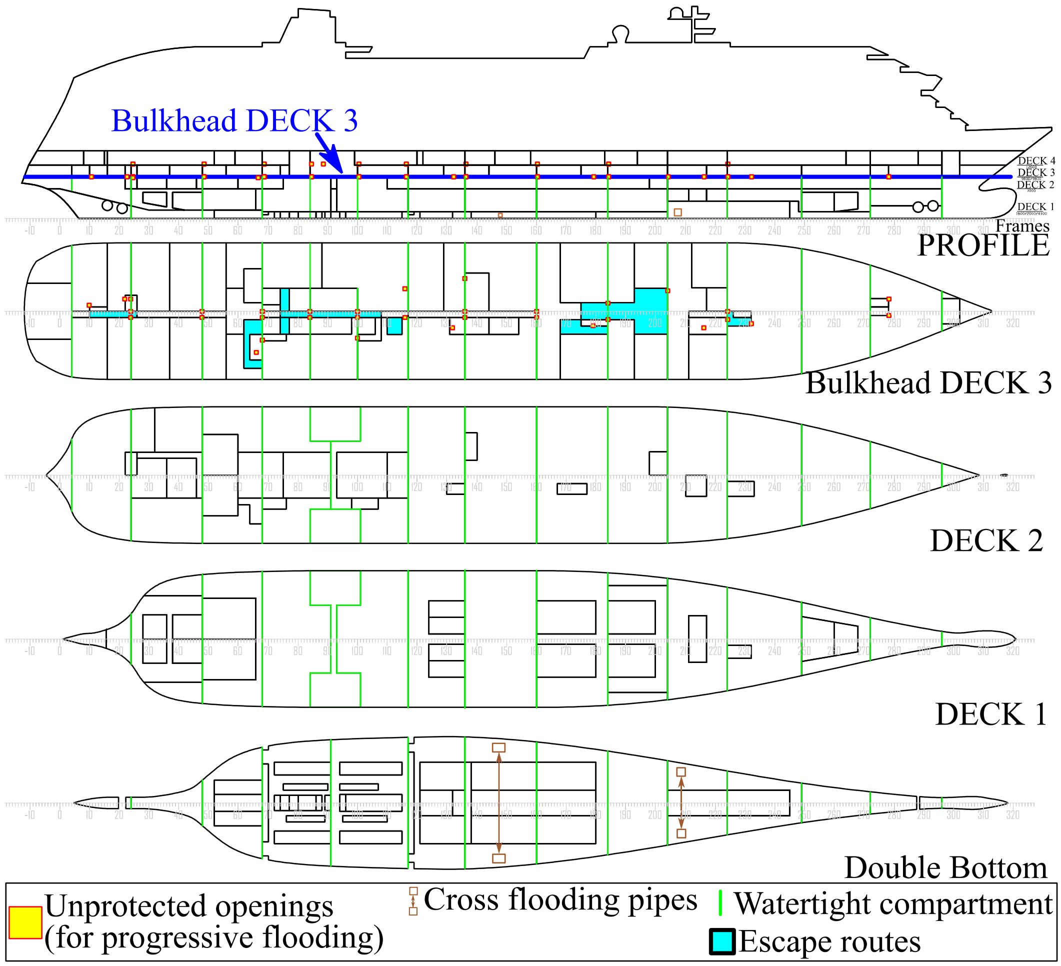

Fig. 11. Passenger vessel watertight subdivision, cross flooding pipes, and unprotected openings for damage stability calculations.

6.2. Derivation of damage extents distributions

Based on the grounding accident statistics displayed in Fig. 12, damage data were derived from a two-way coupled internal and external mechanics model (Section 3). The rapid FSI grounding dynamics method used in this work was numerically validated against LSDYNA-MCOL simulations [28]. For completeness, a brief discussion of the FSI approach employed for deterministic generation of damage extents is presented in Appendix A. Ship survivability assessment relies on the location and extents (longitudinal, transverse, vertical) of damage. For validation purposes, results from numerical simulations were compared against the damage extents of the historical grounding data EMSA [35,36]. Fig. 14 illustrates a summary of the statistics based on EMSA data sets and Monte Carlo simulations utilizing the deterministic crashworthiness FSI technique introduced in this paper (see Section 5.2). Comparisons are based on probability distributions corresponding to available data sets (i.e., *All-types of vessels* and *passenger vessel*). It is shown that the center of damage (η_{dam}) from historical data (Fig. 14a) follows uniform distribution. On the other hand, the deterministic model shows a bimodal distribution (Fig. 14 b and c), with a mean of around ±0.29. Damage length, breadth, and penetration are normalized by the length between the ship's perpendicular L_{PP}, beam of the ship B and potential penetration factor $L_{z,p,max}(B) = L_{z,max}(B) = \min\{0.503*B^{0.636}, T\}$, respectively.

The bimodal distribution could be attributed to FSI deterministic damage extents, for which the center of the damage (Y_{dam}) varies as ship dynamics account for motions in 6-DoF (see Fig. 6, Fig. 8 and Appendix A). Furthermore, the hull bottom limits $b(X_F, z^*)$ are different from the bow to the forebody of the ship. Amidships this limit tends to be equal to the ship's breadth. The location of the rock (Y_{GR}) is uniformly distributed. According to Equation (5), the value of η_{dam} forms a distribution with two peaks. The ESMA distribution, on the other hand, explicitly considers a uniform distribution for the value of the nondimensional center of measured damage η_{dam}.

Figure 15,[2] illustrates the distribution of damage extent statistics. The mean result of the damage length (L_x) from the rapid FSI solver is 55 % higher than the EMSA historical data set. On the other hand, the rapid FSI method shows a decrease in the mean value of damage width (L_y) and penetration (L_z). When considering passenger vessel input distribution, the damage width and penetration shows approximately 28 % lower mean in comparison to historical data. The correlation between the mean and median values of damage extents suggests right-skewed data with a larger tail at the upper end, since the mean is greater than the median. Moreover, the median of the extent of deterministic damage is higher than that of historical data. From an overall perspective, it appears that passenger ship input conditions result in significantly greater mean values for damage width (80 %) and penetration (72 %) than non-passenger input conditions. Furthermore, there is not much of

[2] The box is constructed by dividing the data segments into the lower quartile (corresponding to 25 % of the data), the higher quartile (corresponding to 75 % of the data) and the median value (50 % of the data) as shown by a red line inside the box Fig. 15. The remainder of the data is represented by dashed lines extending from either side of the box, as well as outliers (see the " + " sign). The lines are extended (see "—" lines outside the box) until they reach 1.5 times the interquartile range in each direction.

Table 1
Input probability density functions of ship operating conditions and environmental conditions.

pdf	Passenger vessel	All-types of vessel
Input rock eccentricity pdf. Passenger ships and all-types of vessels. Location of the rock from ship centerline Y_{GR} is in meter		
Eccentricity $x = Y_{GR}$	Uniform distribution $f(x) = \frac{1}{b-a}$	
parameters	$x \in [a, b]; a = -B/2, b = B/2$	
Velocity pdf before grounding event. Passenger ships and all-types of vessels. Impact velocity V_i is normalized by service speed V_s.		
pdf	Passenger vessel	All-types of vessel
Velocity $x = \frac{V_i}{V_s}$	Normal distribution $f(x;\mu,\sigma) = \frac{1}{\sigma\sqrt{2\pi}} e^{-\frac{(x-\mu)^2}{2\sigma^2}}$	Weibull 3-Parameter $f(x;\alpha,\beta,\gamma) = \frac{\beta}{\alpha}\left(\frac{x-\gamma}{\alpha}\right) e^{-\left(\frac{x-\gamma}{\alpha}\right)^{\beta}}$
parameters	$\mu = 0.5489, \sigma = 0.2854 x \in [0.08824, 1]$	$\alpha = 6.526, \beta = 1.697, \gamma = -0.967 x \in [0.01622, 1]$
Input initial rock height above keel line (rock depth) pdf before grounding event.. Passenger ship and all-types of vessel. The depth of the rock D_p is normalized by draft T of the ship		
pdf	Passenger vessel	All-types of vessel
Penetration $x = \frac{D_P}{T}$	Normal distribution $f(x;\mu,\sigma) = \frac{1}{\sigma\sqrt{2\pi}} e^{-\frac{(x-\mu)^2}{2\sigma^2}}$	Gamma 2-Parameter $f(x;\alpha,\beta) = \left(\frac{x^{\alpha-1} e^{-\left(\frac{x}{\beta}\right)}}{\beta^{\alpha}\Gamma(\alpha)}\right)$
parameters	$\mu = 0.1333, \sigma = 0.08523 x \in [0, 0.5]$	$\alpha = 1.313, \beta = 0.06 x \in [0, 0.5]$
Input rock tip radius pdf. Passenger ships and all-types of vessels. Tip radius R_R is normalized by ship breadth B		
pdf	Passenger vessel	All-types of vessel
Tip-Radius $x = \frac{R_R}{0.125B}$	Normal distribution $f(x;\mu,\sigma) = \frac{1}{\sigma\sqrt{2\pi}} e^{-\frac{(x-\mu)^2}{2\sigma^2}}$	Lognormal distribution $f(x;\mu,\sigma) = \frac{1}{x\sigma\sqrt{2\pi}} e^{-\frac{(\log(x)-\mu)^2}{2\sigma^2}}$
parameters	$\mu = 0.1747, \sigma = 0.1112 x \in [0, 1]$	$\mu = -2.41, \sigma = 0.8893 x \in [0, 1]$
Input rock semi-apex angle pdf. Passenger ships and all-types of vessels. Semi apex angle ϕ is in degrees.		
pdf	Passenger vessel	All-types of vessel
Apex-angle $x = 70 - \phi$	Exponential distribution $f(x;\mu) = \frac{1}{\mu} e^{-\frac{x}{\mu}}$	Exponential distribution $f(x;\mu) = \frac{1}{\mu} e^{-\frac{x}{\mu}}$
parameters	$\mu = 10.6094 x \in [0.001, 65]$	$\mu = 12.0837 x \in [0.001, 65]$

a difference between deep and shallow water conditions.

The conventional approach to historical data distributions assumes *"potential damage"* characteristics, where the extent of damage could outspread beyond the domain of the ship. An illustration of the box-shaped damage formed by historical data set and numerical simulations is explained in Fig. 16. The boxes represent the region of damage to the bottom hull. Some of the hull breaches from the database of accidents do not encounter the hull. Although historical breaches are derived from real damage statistics, when these distributions are associated with a specific ship, damage dimensions may extend outside the ship's domain. However, when the deterministic approach is used, no contact is outside the hull domain. The present method maintains a realistic damage profile, as we do not expect the damage to be outside the domain of the ship.

The integration of the deterministic approach leads to realistic detection of damaged and flooded compartments. Since the extent of damage also depends on the type of vessel, structural details, navigational attributes, and maneuvering characteristics, the numerical simulation allows for the specification of alternative material properties and for the assessment of the surrounding environment. This is an advantage since variations of the environmental conditions are not considered when historical data sets are used and changing the subdivision of the ship (bulkheads and compartments) may result in a varied A-index depending on the group(s) of flooded compartments.

The maximum likelihood estimate (MLE) approach was used to fit the damage extents derived from rapid FSI numerical simulations [66]. For the four distinct scenarios outlined in section 5.2, the nondimensional center of location of the rock was fit with a bimodal distribution. For the rest of the damage dimensions a Weibull distribution was used.

Equations (7) and (8) describe the fitted bimodal and Weibull probability density functions, respectively.

$$\textbf{Bimodaldistribution}: f(x;p,\mu_1,\sigma_1,\mu_2,\sigma_2) = \frac{p}{\sigma_1\sqrt{2\pi}} e^{-\frac{(x-\mu_1)^2}{2\sigma_1^2}} + \frac{(1-p)}{\sigma_2\sqrt{2\pi}} e^{-\frac{(x-\mu_2)^2}{2\sigma_2^2}} \tag{7}$$

$$\textbf{Weibulldistribution}: f(x;\alpha,\beta) = \frac{\beta}{\alpha}\left(\frac{x}{\alpha}\right)^{\beta-1} e^{-\left(\frac{x}{\alpha}\right)^{\beta}} \tag{8}$$

where, μ and σ are the mean and standard deviations of the normal distribution; α *and* β are scale and shape factors. Table 2, contains the parameters of the fitted pdfs, and Appendix B demonstrates histograms of the damage extents from numerical simulations and fitted distributions.

6.3. Distribution of maximum forces, deformation energy and ship motions

Structural failure loads and ship motion amplitudes were attained from numerical ship grounding simulations accounting for the external dynamics conditions, shown in Table 3. The details of the histogram and fitted distributions of the maximum grounding forces for four cases are given in Appendix C. It was found that the numerically simulated longitudinal resistance force has a generalized extreme value distribution (Equation (9)). On the other hand, the vertical and transversal structural resistance values display a log-logisticic distribution (Equation (10)). The maximum total deformation energy of the structure shows a gamma distribution (Equation (11)).

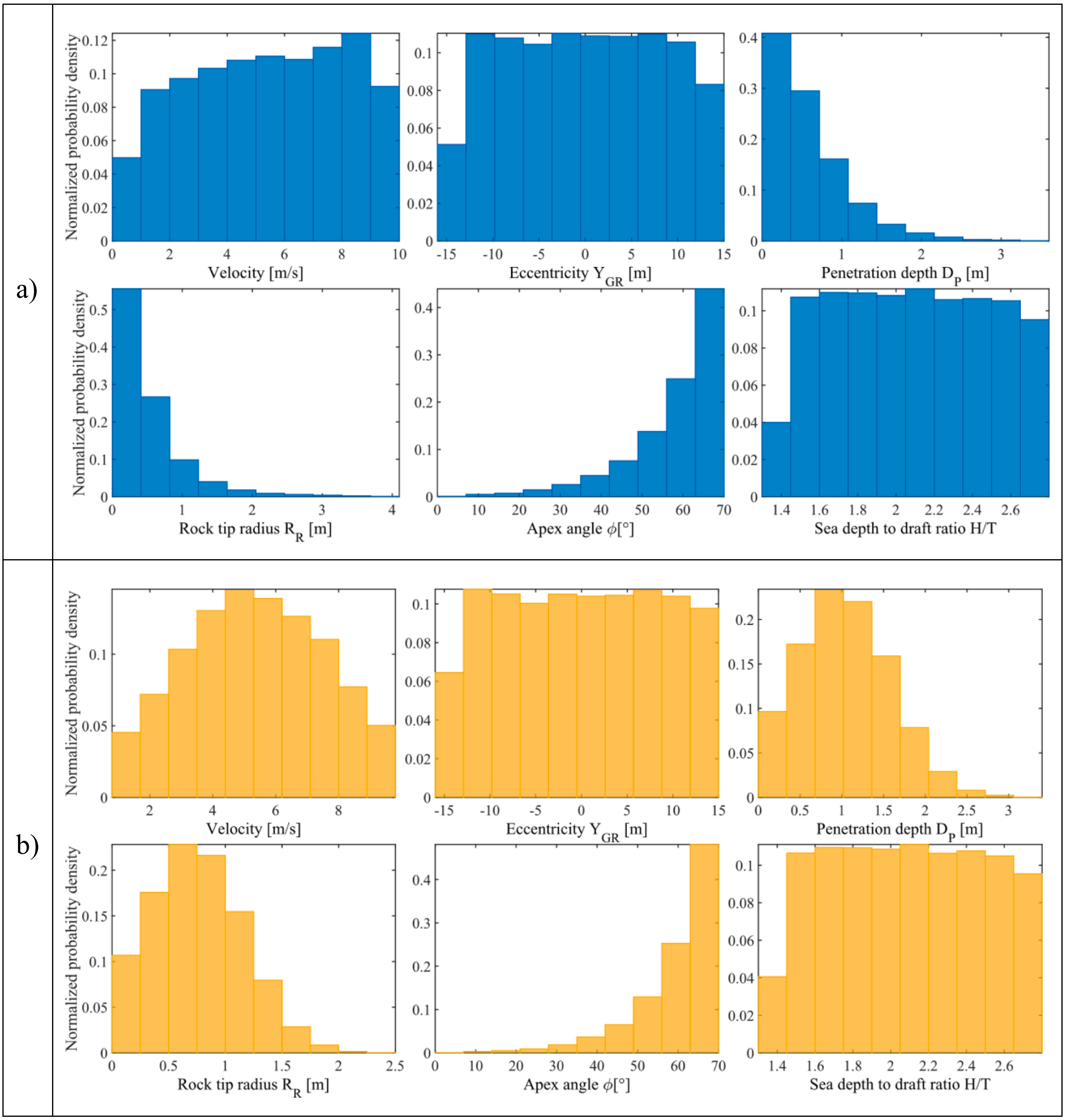

Fig. 12. Input values for stochastic grounding simulation. Random samples generated from the input probability distribution a) All-types vessel and b) Passenger vessels distributions.

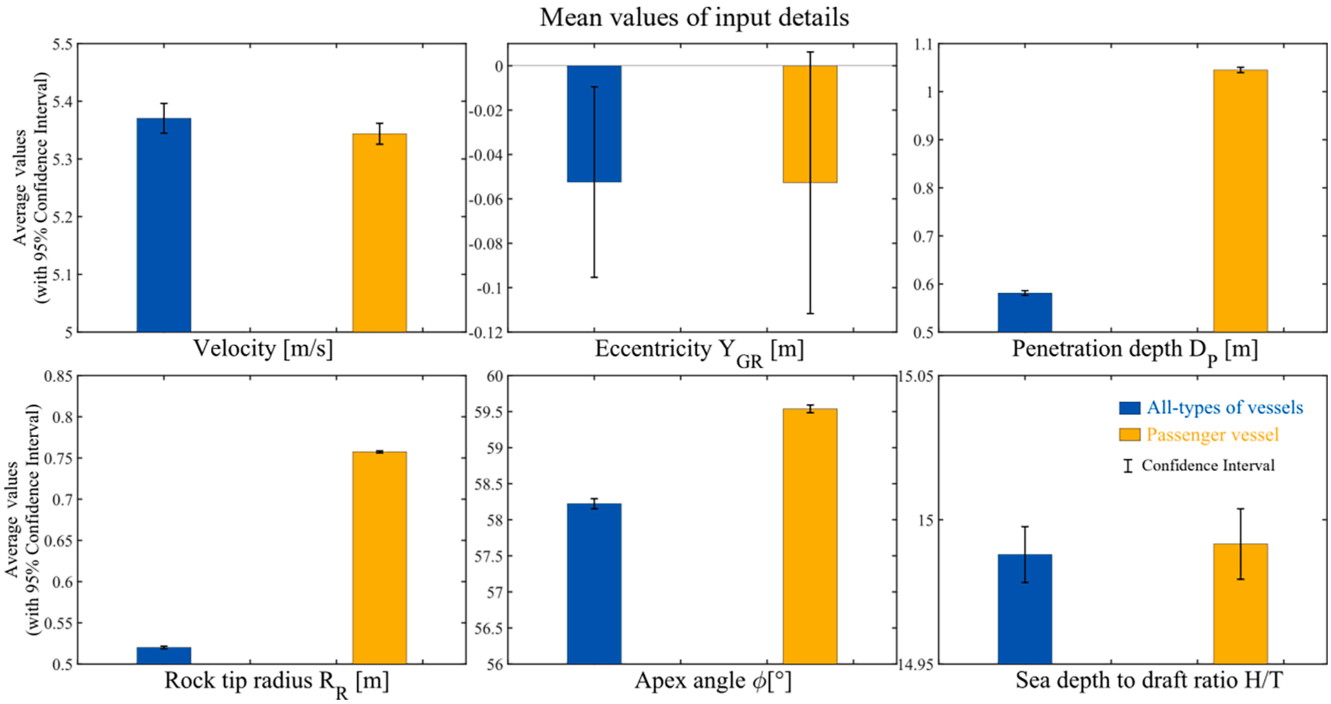

Fig. 13. Average values of the input probability distribution.

The statistical assessment of the mean value of the structural grounding forces and amplitudes of the ship with 95 % confidence interval is shown in Fig. 17. Compared to *All-types of vessel* (Table 1), *passenger vessel* input pdfs were shown to have substantially higher mean values of structural resistance forces and ship amplitudes (the resistance force is 2.5 to 4.5 higher and the ship amplitude is 1.5 to 2 times higher). This may be attributed to the depth of penetration of the rock, which has a lower mean value in the *all types of vessels* data set (see Fig. 13).

In deep-water conditions, there is a very minor increase in grounding forces and ship amplitudes. This could be attributed to the ship's resistance, which is somewhat higher in shallow waters. Table 3 summarizes the statistics on grounding forces and ship motions. After fitting the distributions, a nonparametric (Wilcoxon rank-sum) test was carried out to validate the fitted population distributions against the grounding samples. This represents the fitted pdfs for the cases of the structural resistance force, ship motions and deformation energy (see Appendix C and D).

$$\textbf{GeneralizedExtremeValuedistribution}: f(x;\xi,\mu,\sigma) = \frac{1}{\sigma}\exp\left(-\left(1+\xi\left(\frac{x-\mu}{\sigma}\right)\right)^{-\frac{1}{\xi}}\right)\left(1+\xi\left(\frac{x-\mu}{\sigma}\right)\right)^{-\frac{1}{\xi}-1} \tag{9}$$

$$\textbf{Log-logisticdistribution}: f(x;\mu,\sigma) = \frac{e^{\left(\frac{\log(x)-\mu}{\sigma}\right)}}{\sigma x}\left(1+e^{\left(\frac{\log(x)-\mu}{\sigma}\right)}\right)^{-2} \tag{10}$$

$$\textbf{GammaDistribution}: f(x;\alpha,\beta) = \left(\frac{x^{\alpha-1}e^{-\left(\frac{x}{\beta}\right)}}{\beta^{\alpha}\Gamma(\alpha)}\right) \tag{11}$$

$$\textbf{Half-NormalDistribution}: f(x;\mu,\sigma) = \frac{2}{\sigma\sqrt{2\pi}}e^{-\frac{1}{2}\left(\frac{x}{\sigma}\right)^2} \tag{12}$$

$$\textbf{LognormalDistribution}: f(x;\mu,\sigma) = \frac{1}{x\sigma\sqrt{2\pi}}e^{-\frac{(\log(x)-\mu)^2}{2\sigma^2}} \tag{13}$$

$$\textbf{BurrTypeXIIDistribution}: f(x;\lambda,c,k) = \frac{\frac{kc}{\lambda}\left(\frac{x}{\lambda}\right)^{c-1}}{\left(1+(x/\lambda)^{c}\right)^{k+1}} \tag{14}$$

6.4. Calculation of the A-index

The ship's survivability level in the event of a grounding is expressed as the A-index of Equation (3). This value determines if the vessel can withstand certain damages while still ensuring the safety of the crew and passengers. In order to calculate the A-index, we must consider damaged compartments which are flooded. In bottom grounding scenarios floodwater progresses upwards through hull internal openings such as staircases and trunks (see Fig. 11). Therefore, most onerous design assumptions consider all rooms in the same watertight compartment to be flooded simultaneously. Cross-flooding in the double bottom void spaces may be considered for damage cases where only one side of the connection is breached. In this study, for each damage case, the *s*-factor was calculated according to SOLAS Ch. II-1, considering also escape routes. Progressive flooding along the bulkhead deck was not considered, and instead, immersion of such openings was accounted for in the evaluation of the *s*-factor.

Damage stability analysis was performed for the design draft condition using damage extents acquired from the deterministic FSI Monte Carlo simulations. The attained index was obtained separately for 4 different impact scenarios, under realistic conditions with 95 % confidence interval (see Fig. 18). Additionally, a comparison is also made with the attained index from a historical dataset [36]. The difference between deep and shallow water conditions is not substantial. However, the confidence interval is a little wider in the case of shallow water. This illustrates the additional variability in the sample due to the influence of increased resistance of the ship and can be reduced by increasing the number of simulations to get closer to the population mean. Another important finding is that of the historical damage distribution (EMSA-grounding dataset Fig. 18), where the attained index is much lower than numerically estimated FSI results. However, this is not particularly surprising given that the historical data distributions overestimate the horizontal and vertical extent of damage (Figs. 15 and 16). Furthermore, it should be noted that this applies just to the studied case (FLOODSTAND SHIP B) and does not necessarily apply to other ships.

Notwithstanding the above, it is obvious that input conditions based on vessel statistics (in this case passenger vessels) may yield a different

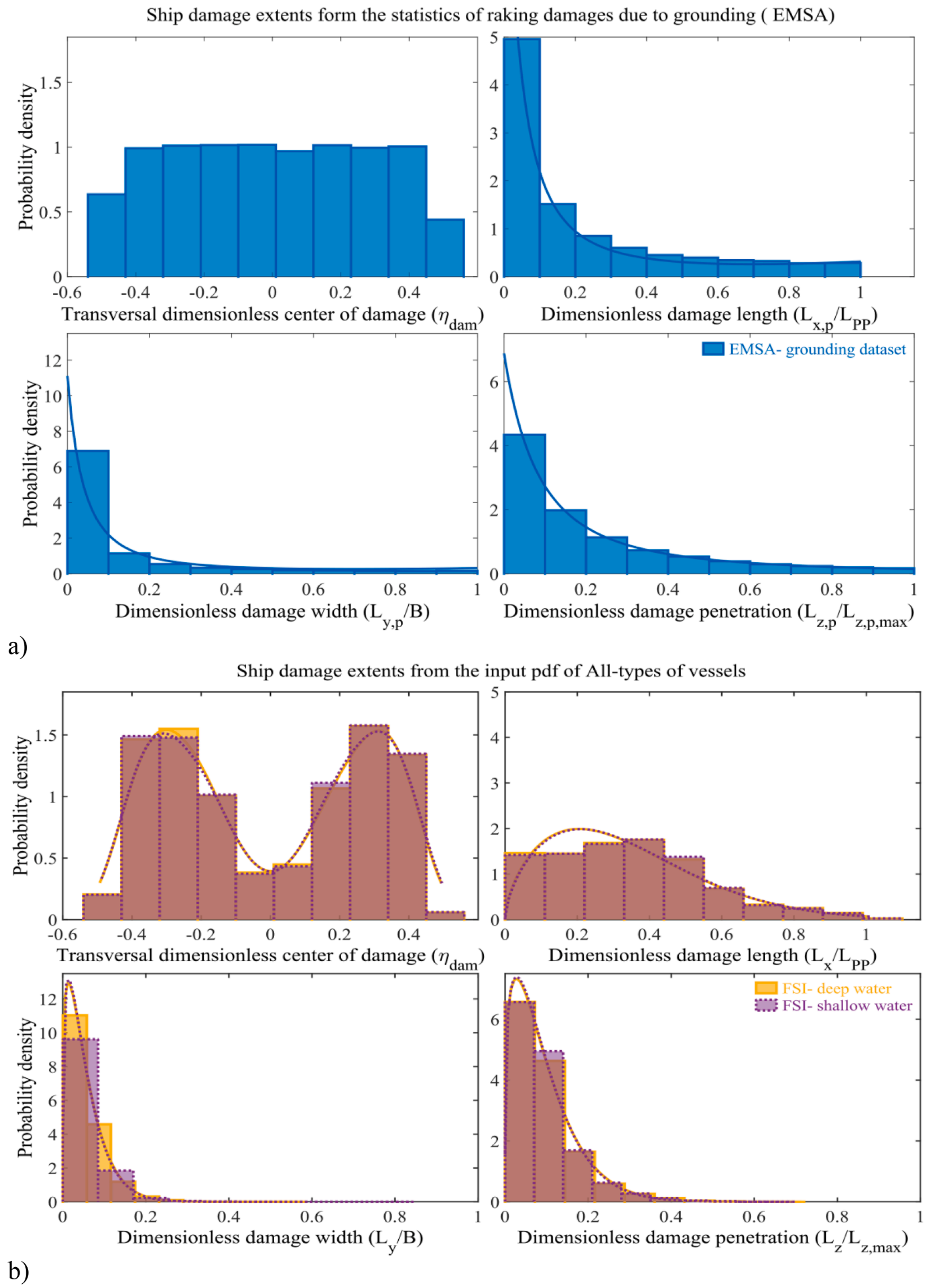

Fig. 14. Non-dimensional output of probability density function. (a) Damage extents from historical data set of EMSA [36]; (b) Damage extents from the input distribution of All-Types of vessels, and (c) Damage extents from the input distribution of passenger vessels.

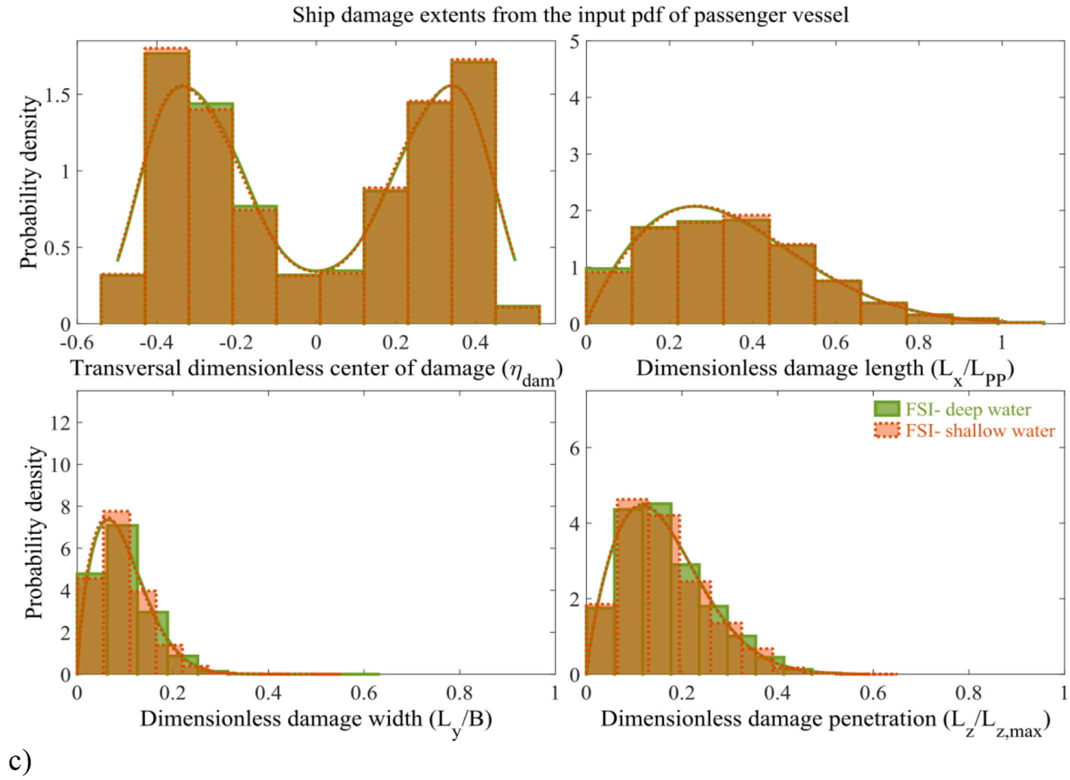

Fig. 14. (*continued*).

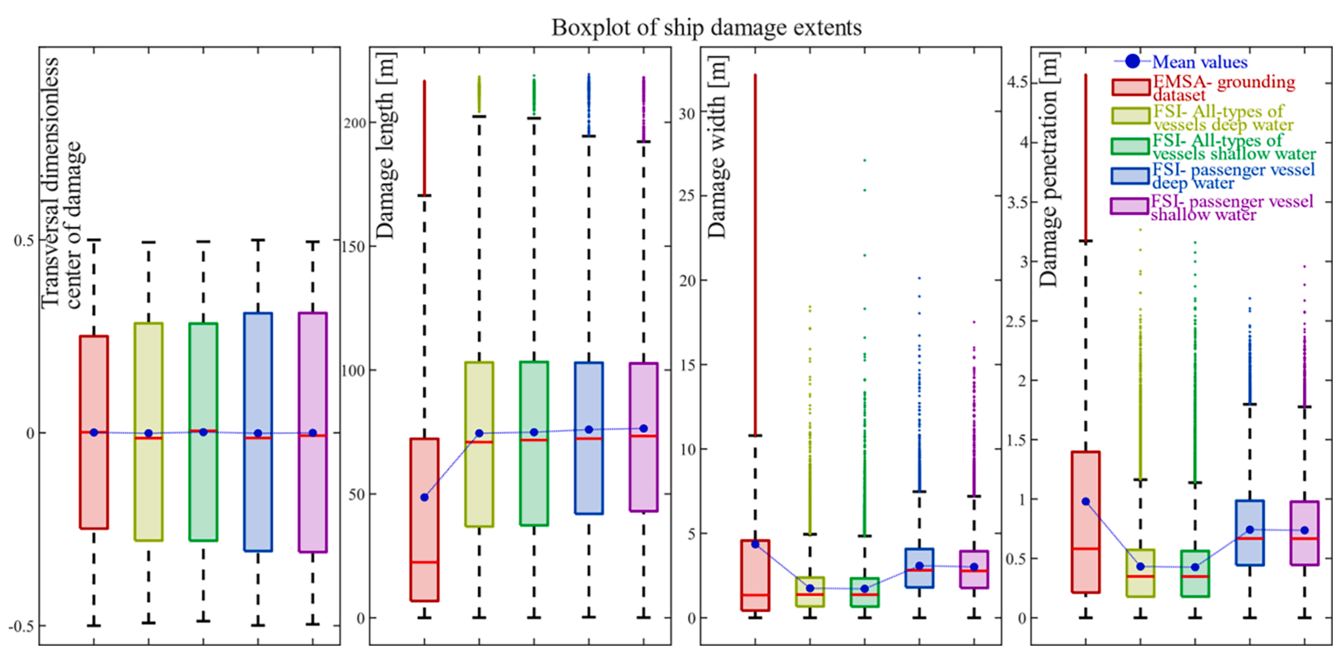

Fig. 15. Box plots of damage extents computed from different probability density functions in deep and shallow water, and details from historical data.

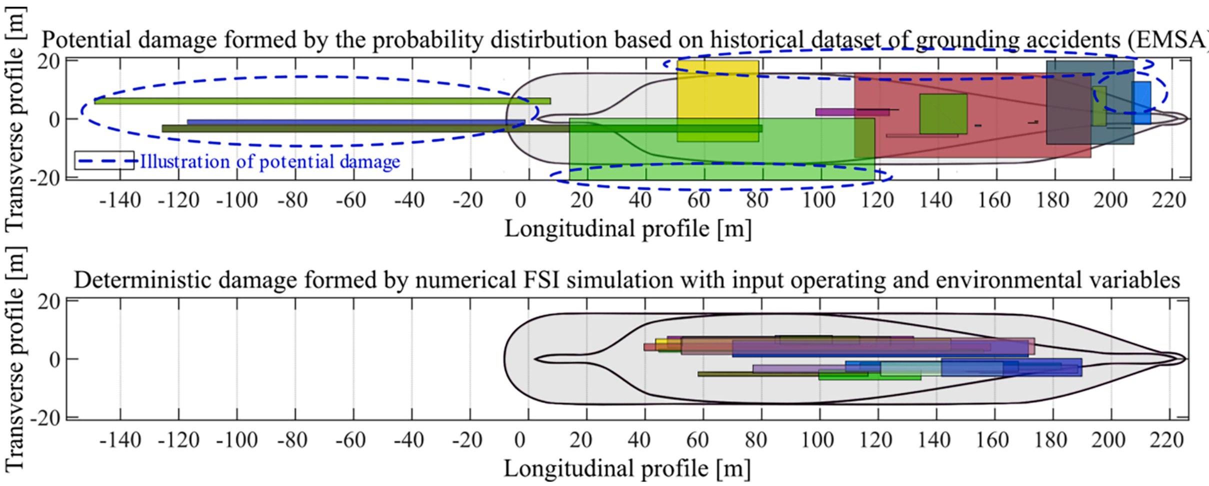

Fig. 16. Illustrations of damage extent distributions according to historical data and FSI simulations. The dashed encircled region shows potential damage, where the extent of damage is outside the ship domain.

Table 2
Characteristics of the numerically simulated damage extent fitted with selected pdf.

Variables		All-types of vessel Input Distribution		Passenger vessel Input Distribution	
		Deep water	Shallow water	Deep water	Shallow water
$-0.5 \leq \eta_{dam} \leq 0.5$Bimodal	p	0.5048	0.4999	0.5049	0.5024
	μ_1	−0.2678	−0.2681	−0.2893	−0.2909
	μ_2	0.2709	0.2714	0.2929	0.2934
	σ_1	0.1088	0.1098	0.1094	0.1099
	σ_2	0.1087	0.1088	0.1091	0.1081
$0.06 \leq L_X \leq 220$**(m)**	α	82.7427	83.2484	85.5418	86.0419
Weibull	β	1.5925	1.6083	1.8515	1.8824
$0.0005 \leq L_Y \leq 27.1$**(m)**	α	1.8666	1.8302	3.4517	3.3751
Weibull	β	1.2068	1.2020	1.7340	1.7091
$0.0001 \leq L_Z \leq 3.3$(**m**)Weibull	α	0.4636	0.4585	0.8325	0.8261
	β	1.2432	1.2520	1.8190	1.8244

Table 3
Characteristics of the numerically simulated maximum grounding forces and maximum ship motions fitted with select pdf.

Variables	All-types of vessel Input Distribution Deep waters	Shallow waters	Passenger vessel Input Distribution Deep waters	Shallow waters	
$0.003 \leq F_X \leq 120$(MN)*GeneralizedExtremeValue*	ξ	0.6061	0.6014	0.6472	3.8819
	μ	1.5687	1.5727	0.6457	3.8859
	σ	2.1647	2.1748	0.6472	3.8819
$0.0001 \leq F_Y \leq 71$(*MN*)Log-logistic	μ	−2.5278	−2.5428	−1.1224	−1.1429
	σ	1.0085	1.0006	0.9393	0.9261
$0.01 \leq F_Z \leq 365$(*MN*)Log-logistic	μ	1.4992	1.5046	2.1602	2.1571
	σ	0.3551	0.3566	0.5523	0.5522
$0.1 \leq E_{Def} \leq 1695$(*MJ*)Gamma	α	0.68	0.70	1.04	1.05
	β	226.37	214.74	263.80	262.40
$0 \leq$ ***Heave*** ≤ 5.9(*m*)Lognormal	μ	−2.9065	−2.9119	–	–
	σ	0.8720	0.8732	–	–
$0 \leq$ ***Heave*** ≤ 0.8(*m*)Weibull	α	–	–	0.1644	0.1637
	β	–	–	1.5953	1.5891
$0 \leq$ ***Roll*** $\leq 47(^\circ)$***GeneralizedExtremeValue***	ξ	0.5154	0.5006	–	–
	μ	0.6813	0.6838	–	–
	σ	0.7075	0.7121	–	–
$0 \leq$ ***Roll*** $\leq 17(^\circ)$***Halfnormal***	μ	–	–	3.7200	3.6515
$0 \leqslant$***Pitch***$\leqslant 12.5$ $(^\circ)$***Burr Type XII***	λ	0.0336	0.0299	0.3961	0.3980
	c	1.4452	1.5229	1.1903	1.1831
	k	1.2419	1.1149	5.9175	5.9394
$0 \leq$ ***Yaw*** $\leq 200(^\circ)$***BurrTypeXII***	λ	9.1198	4.7616	4847.6680	12.7788
	c	0.7689	0.7988	0.8930	0.9758
	k	5.9728	4.0276	989.6583	7.2762

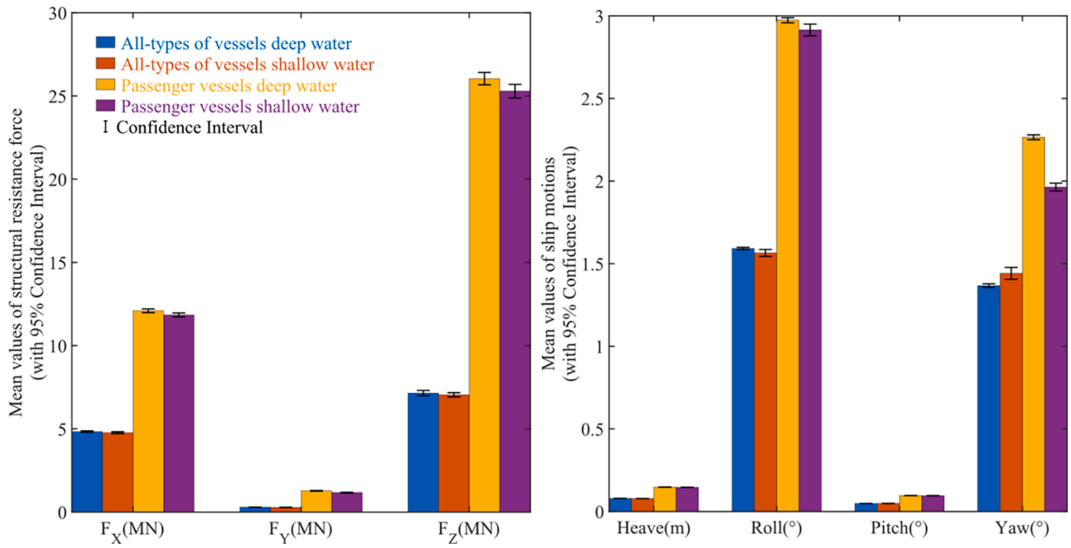

Fig. 17. Mean values of maximum grounding forces and ship amplitudes during a grounding event with a confidence interval of 95%. Comparison of different scenarios under deep and shallow water conditions.

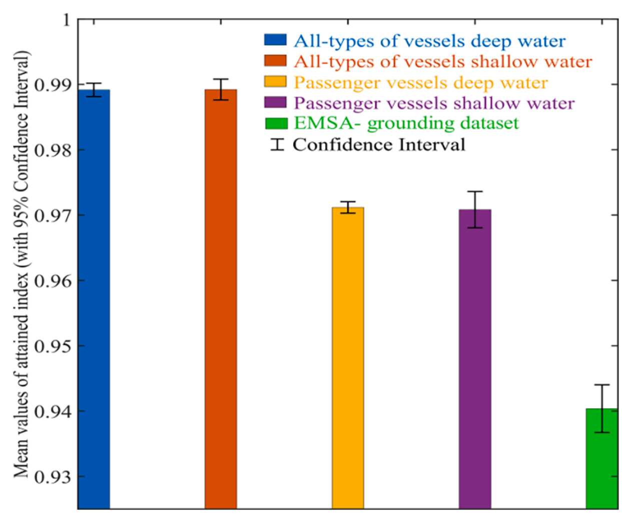

Fig. 18. Passenger vessel attained subdivision index. Four different impacts and surrounding scenarios, and historical data set.

(in this case lower) value of *A*. This is because the penetration height of the rock was 75 % greater for the case of "passenger vessel input" distribution as compared to "All-types of vessel input" distributions (see Fig. 13). As a result, more rooms are penetrated vertically, which means that flooding is not limited to the double bottom, resulting in a significantly lower s-factor and, eventually, a lower *A*. In each case, *A* is notably higher than the required subdivision index (R = 0.8675) as per SOLAS2020 Chapter II-1 Part B-1 Regulation 6.

7. Conclusions

This paper presented a probabilistic method for the assessment of damage extents following ship hard grounding. The method is based on a rapid FSI model that accounts for structural and hydrodynamic topologies, ship dynamics and operational conditions. The new aspect of the method is damage profile modelling, which is based on the so-called actual damages. This means that the damage profile is generated not just inside the ship's domain, but also takes into consideration structural topology, vessel kinematics, environmental forces, and maneuvering motions. The purpose of this approach is to generate realistic probabilistic damage datasets that can be used to assess ship damage stability or structural integrity.

Comparisons of the extents of damage derived from the new method against EMSA historical data records indicated larger estimates of the ship's damage length following grounding. However, the width and penetration depths are predicted to be smaller, and this could be attributed to oversimplified assumptions of historical data *"potential damage"* records. Because of the influence of ship evasiveness, the higher estimation of damage width and penetration depth from historical data may be valid. Notwithstanding this, the historical probabilistic damage estimates did not consider the operating conditions, structural arrangement (single bottom, double bottom, watertight compartments, etc.), and the profile of the seabed.

The model considered only the influence of conical rock profiles, straight-line ship operations and neglected side grounding scenarios. Accordingly, future work could focus on modelling paraboloid forms of rock and ship evasive actions and modelling side grounding damages that may be orthogonal to the vessel's center plane. Such developments could have a significant impact on the development of future IMO SOLAS damage stability regulations and the development of criteria

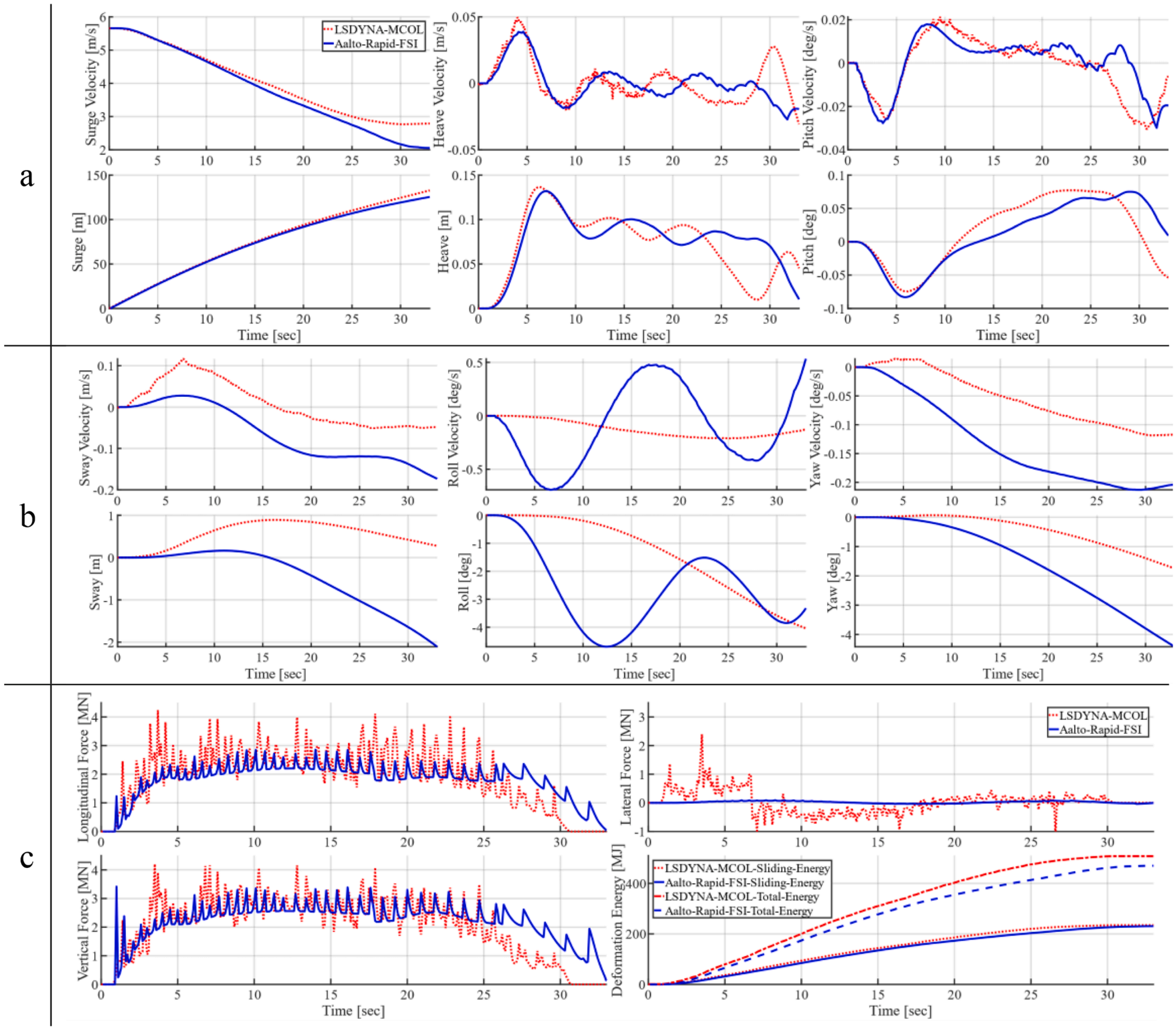

Fig. 19. Side (B/4) grounding of a passenger ship. Velocities, displacements, forces and energy. a) Surge, heave and pitch motions and b) Sway, roll and yaw motions c) Sliding forces and deformation energy of side (B/4) grounding of a passenger ship.

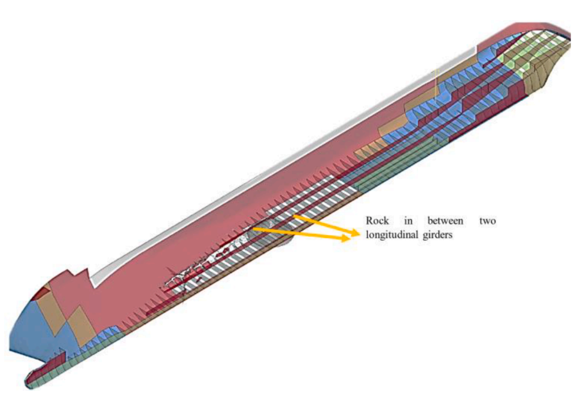

Fig. 20. Off-center grounding LSDYNA-MCOL validation study, rock fastened in between two longitudinal girders.

Table 4
Maximum damage limits of the Off-center passenger ship grounding. Comparison of the present model with LS-DYNA simulations.

	LSDYNA	Present simplified FSI method	% Difference
Longitudinal Extent (m)	119.13	119.8	0.56
Maximum width (m)	5.30	5.08	4.2
Maximum penetration (m)	1.86	1.68	9.7
Inner bottom breach	Yes	Yes	–
Maximum Longitudinal Force (MN)	4.24	2.97	30
Maximum Transverse Force (MN)	2.39	0.10	95
Maximum Vertical Force (MN)	4.20	3.45	18
Maximum Deformation Energy (MJ)	507.4	468.1	7.8
Maximum Heave (m)	0.1366	0.1302	4.7
Maximum Roll (deg)	3.54	4.67	32
Maximum Pitch (deg)	0.075	0.082	9.5
Maximum Yaw (deg)	1.65	3.78	129

implemented in intelligent Decision Support Systems (DSS). The probabilistic model presented in this work is limited to a specific ship design and structural arrangement of a modern passenger vessel. Consequently, future research on situations involving various ship types and structural configurations can assist us in integrating the probabilistic models for damaged ship survivability assessment.

Declaration of Competing Interest

The authors declare that they have no known competing financial interests or personal relationships that could have appeared to influence the work reported in this paper.

Data availability

No data was used for the research described in the article.

Appendix A:. Validation study of an off-center grounding

Results of the off-center (B/4) grounding of the passenger vessel are shown in Fig. 19. The results of the surge, heave, and pitch motions match well with the values available from the validation study. The total length of damage of the ship is the same as that of the ship completely passing over the rock. The surge velocity from the LS-DYNA simulation and the rapid FSI model shows that the contact between the ship and the rock separates after 30.6 and 33.2 s, respectively, which can be seen as a constant surge velocity (see Fig. 19a), after almost 30 s.

The present model shows on average 8.5 % lower values of horizontal resistance in comparison to validation case Fig. 19c. The vertical force is within 3 %, and the trend of the force fits well with the simulations. The variation of vertical force is also realized in heave motion. It has slightly less heave amplitude due to lower force. The difference in the surge velocity corresponds to the lower estimation of the horizontal force in a simplified model.

Significant differences in roll motions are found during grounding. Sway motion is underpredicted (Fig. 19b). The FEM simulation shows that the rock is in between two longitudinal girders, which delays the rolling of the ship and causes a steady increase of the roll motion (see Fig. 20). The underestimation of the transverse force (rock in between two longitudinal girders) by the simplified model leads to higher roll and ultimately affects the swaying and yawing of the ship.

The trend of the sway directional lateral force is different; the average force is within 2 % of the FEM simulation. The total deformation energy and sliding energy are within 10 % and 4 % respectively Fig. 19c.

The largest values in the validation of the simplified FSI method against LSDYNA simulations are shown in Table 4. This shows the details of maximum damage extents, forces, deformation energy, and ship motions of the passenger ship off-center grounding.

Appendix B:. Fitted probability distribution of damage extents

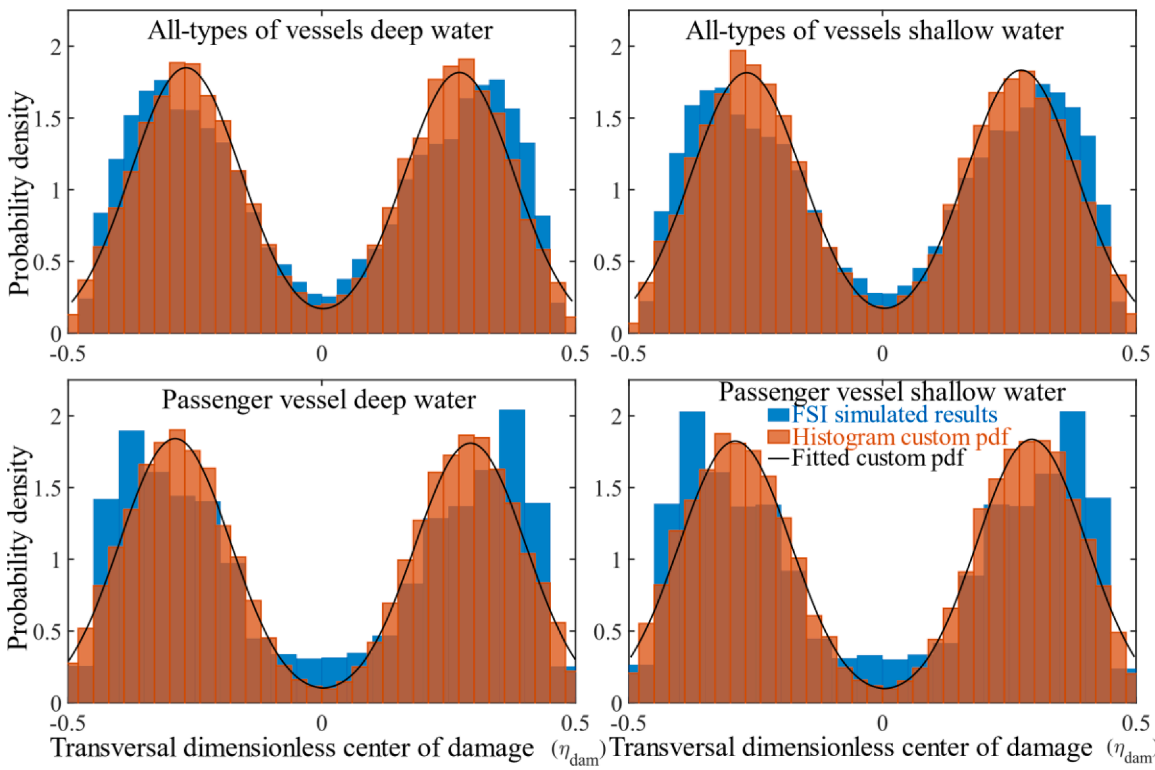

.

a) Fitted bimodal distribution of the dimensionless position of the center of damage η_{dam}. Histograms display numerically calculated deterministic values against fitted pdfs. Input conditions consider deep and shallow waters with operating distributions of *passenger vessels* and *all-types* of vessels.

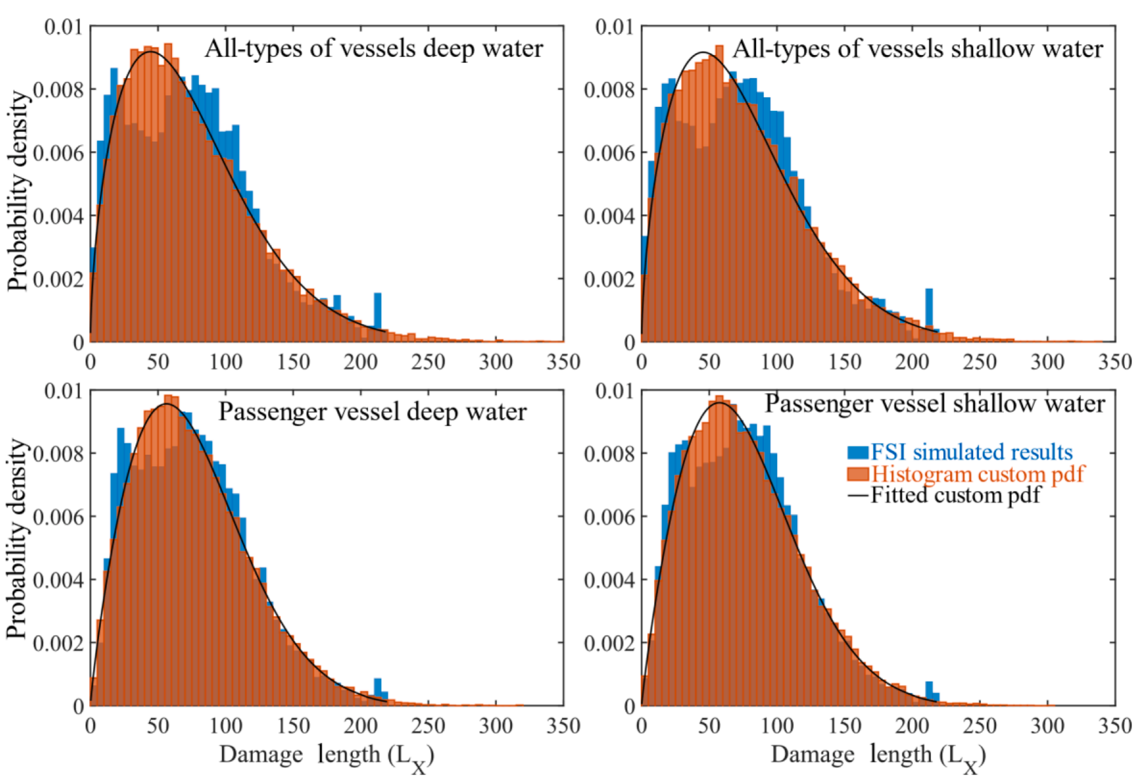

.

b) Fitted Weibull distribution of damage length L_X in meters. Histograms display numerically calculated deterministic values against fitted pdfs. Input conditions consist of deep and shallow water with operating distributions of *passenger* vessels and *all-types* of vessels.

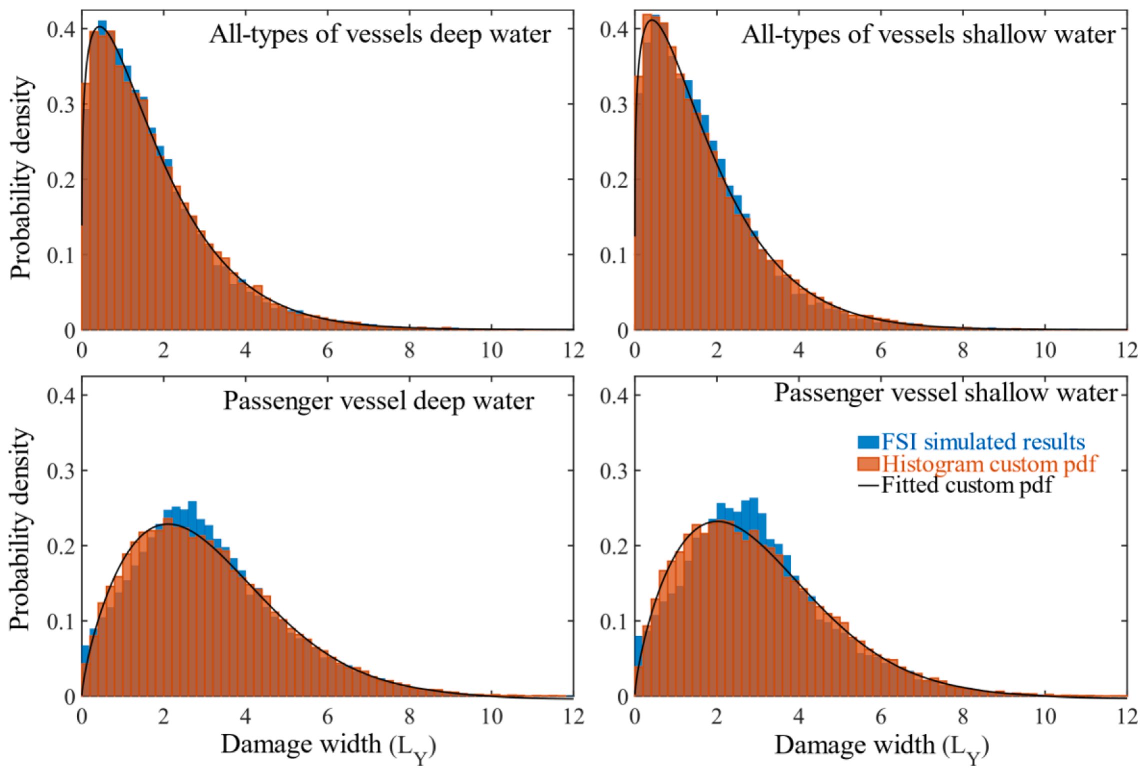

c) Fitted Weibull distribution of damage width L_Y in meters. Histograms display numerically calculated deterministic values against fitted pdfs. Input conditions consist of deep and shallow water with operating distributions of *passenger* vessels and *all-types* of vessels.

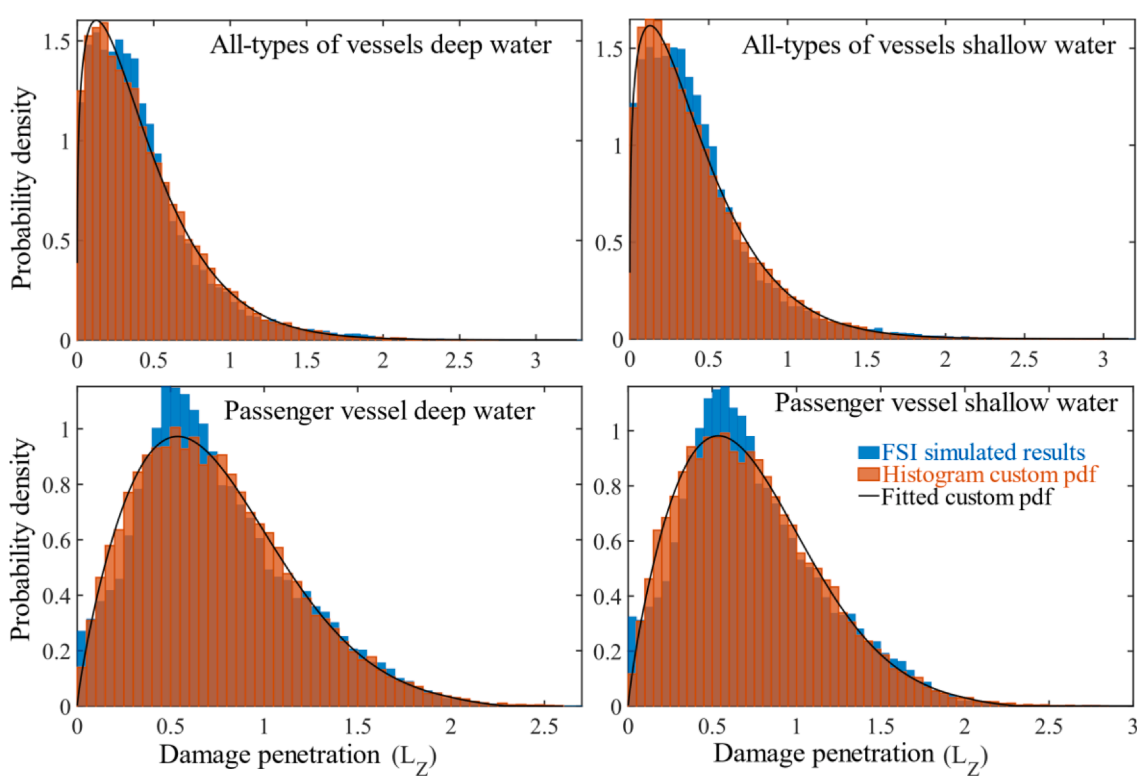

d) Fitted Weibull distribution of damage penetration L_Z in meters. Histograms display numerically calculated deterministic values against fitted pdfs. Input conditions consist of deep and shallow water with operating distributions of *passenger* vessels and *all-types* of vessels.

Appendix C:. Fitted probability distribution of maximum structural resistance force

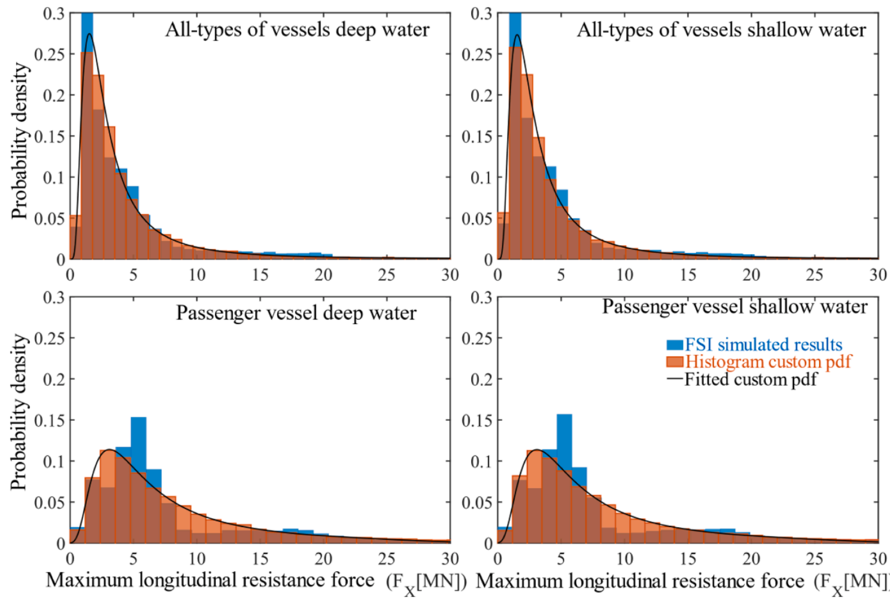

.

a) Fitted generalize extreme value distributions of maximum longitudinal structural resistance forces (MN) during a grounding event. Histograms display numerically simulated grounding forces and fitted pdfs. Input conditions account for deep and shallow waters for both *passenger vessels* and *all-types of vessels*.

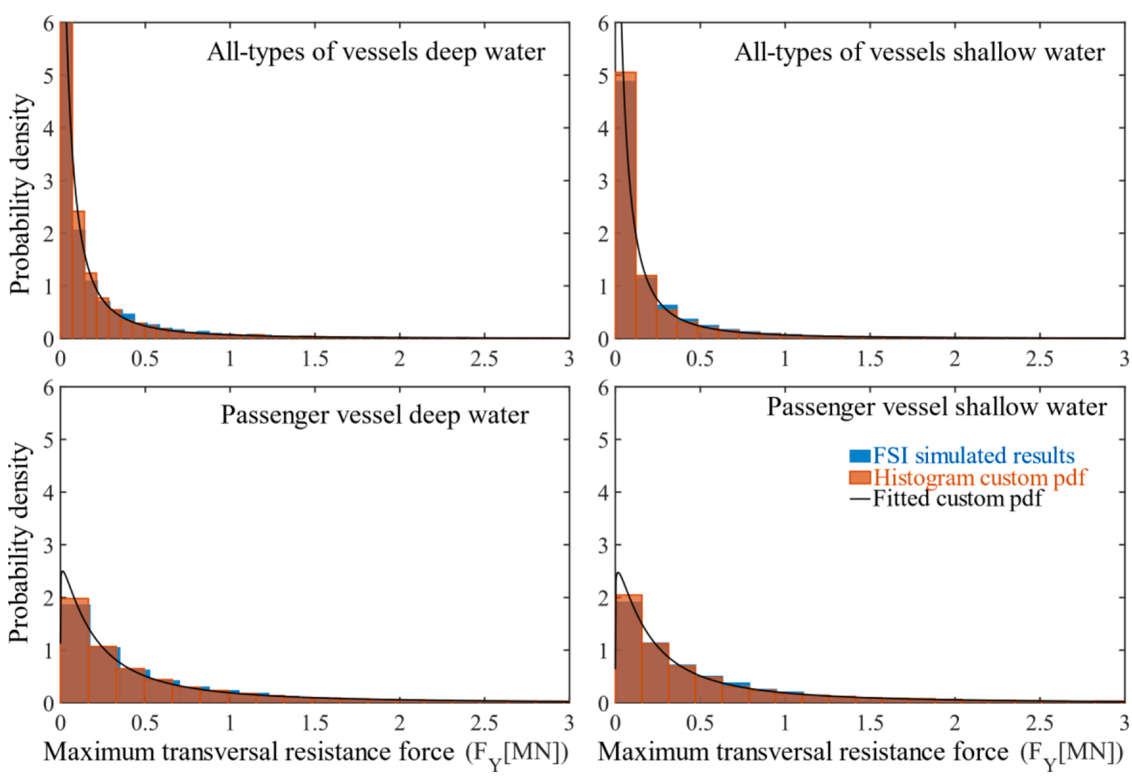

.

b) Fitted loglogistic distribution of maximum transversal structural resistance force (MN) during a grounding event. Histograms display numerically simulated grounding forces and fitted pdfs. Input conditions account for deep and shallow waters for *passenger vessels* and *all-types of vessels*.

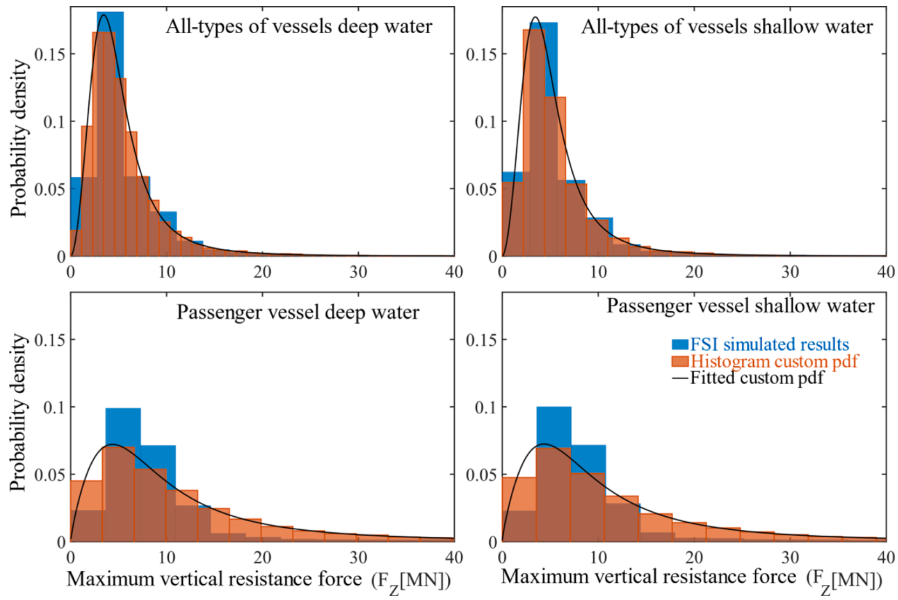

.

c) Fitted log-logistic distribution of maximum vertical structural resistance force (MN) during a grounding event. Histograms display numerically simulated grounding forces and fitted pdfs. Input conditions consider deep and shallow waters with operating distributions of passenger vessels and all-types of vessels.

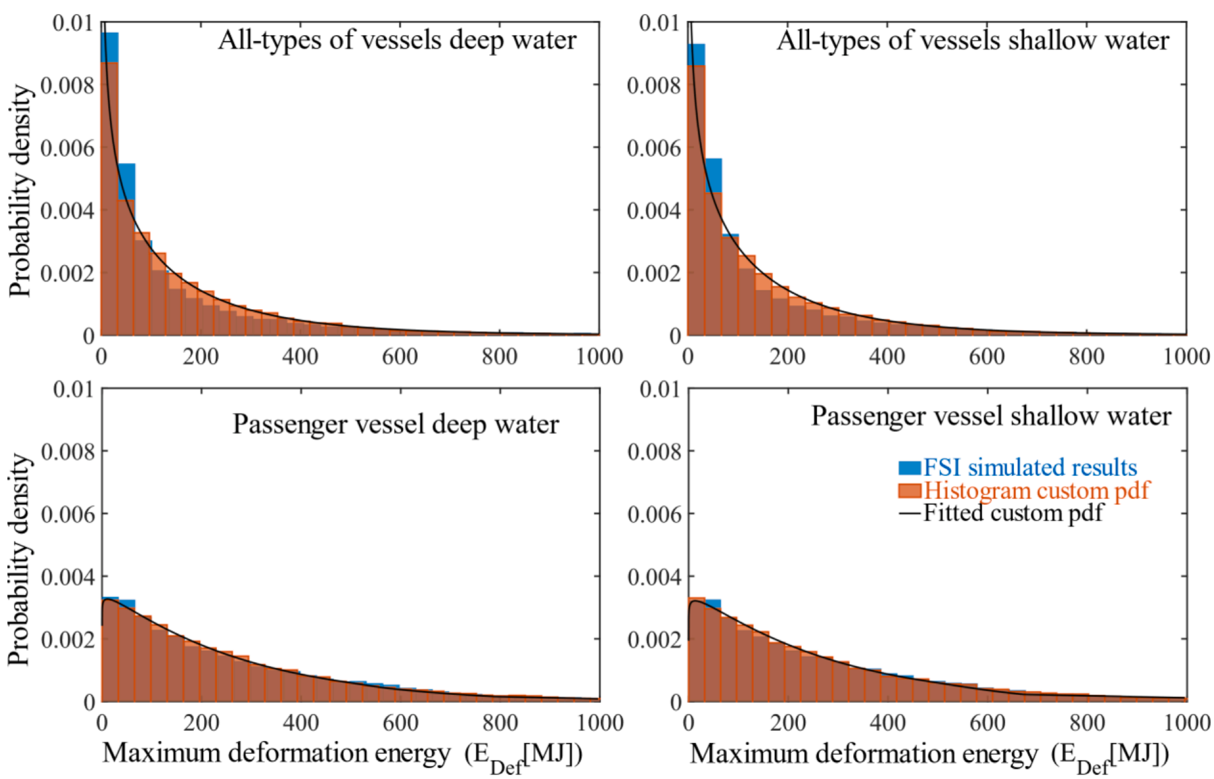

.

d) Fitted gamma distribution of total structural deformation energy (MJ) during a grounding event. Histograms display numerically simulated grounding energy and fitted pdfs. Input conditions consider deep and shallow waters with operating distributions for *passenger vessels* and *all-types of vessels*.

Appendix D:. Fitted probability distribution of maximum ship motions

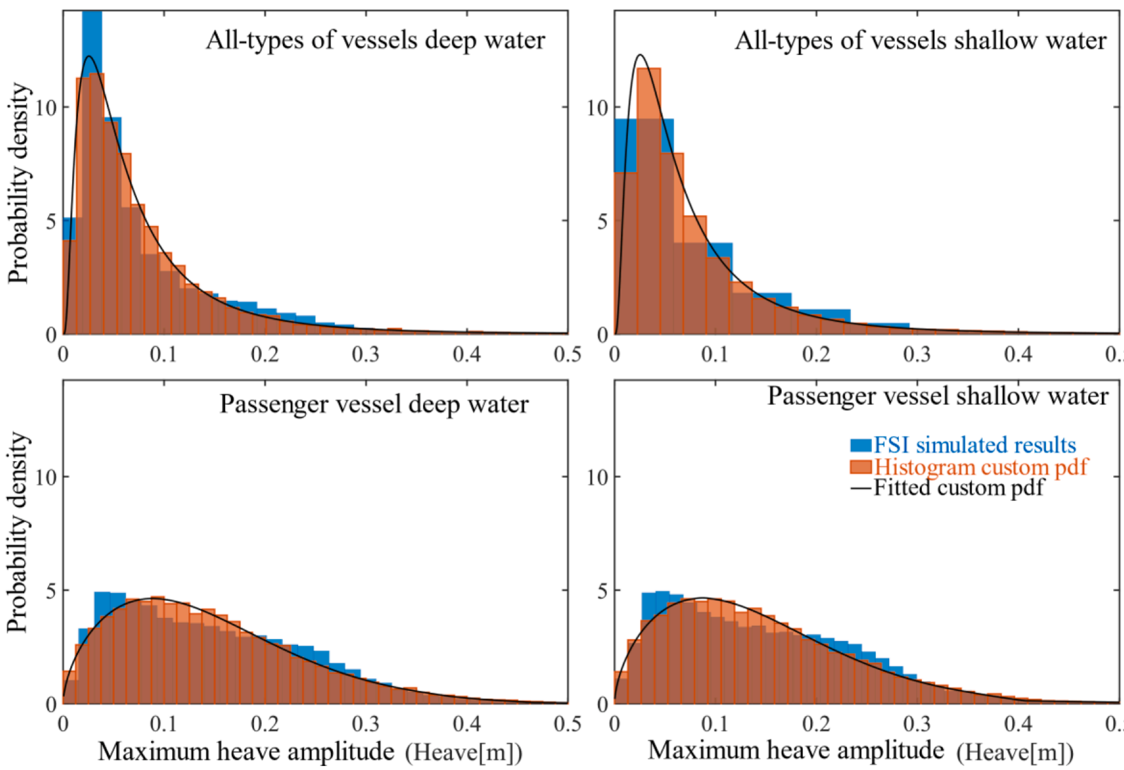

.

a) Fitted lognormal (*All-types of vessels*) and Weibull (*Passenger vessels*) distributions of maximum heave motion during a grounding event. Histograms display numerically simulated grounding ship motions and fitted pdfs.

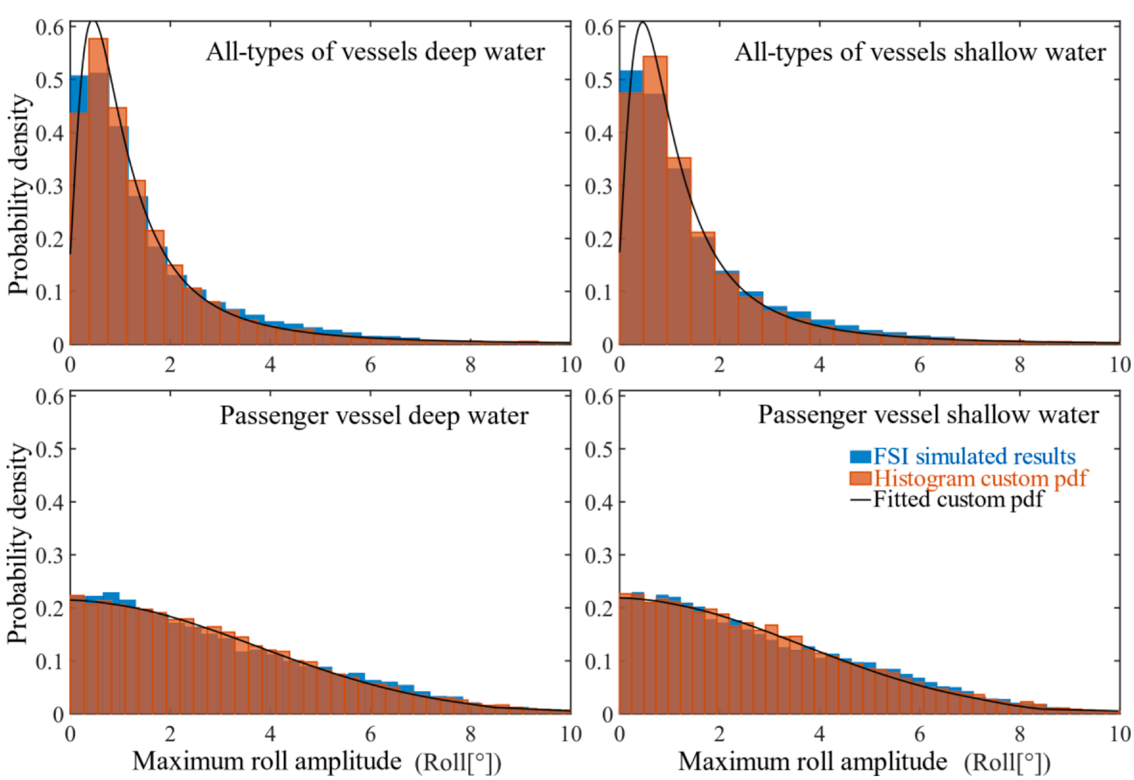

.

b) Fitted generalize extreme value (*All-types of vessels*) and half normal (*Passenger vessels*) distributions of maximum roll motion during a grounding event. Histograms display numerically simulated grounding ship motions and fitted pdfs.

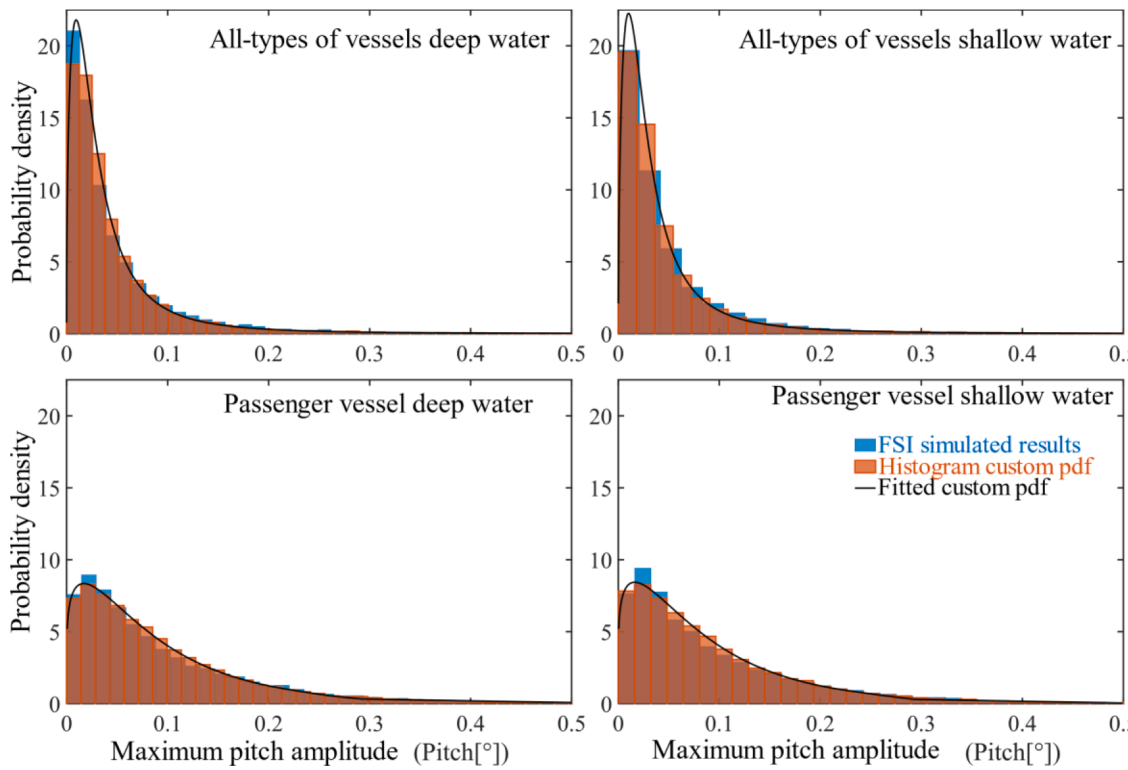

.

c) Fitted Burr type XII distributions of maximum pitch motion during a grounding event. Histograms display numerically simulated grounding ship motions and fitted pdfs. Input conditions account for deep and shallow waters for *passenger vessels* and *all-types of vessels*.

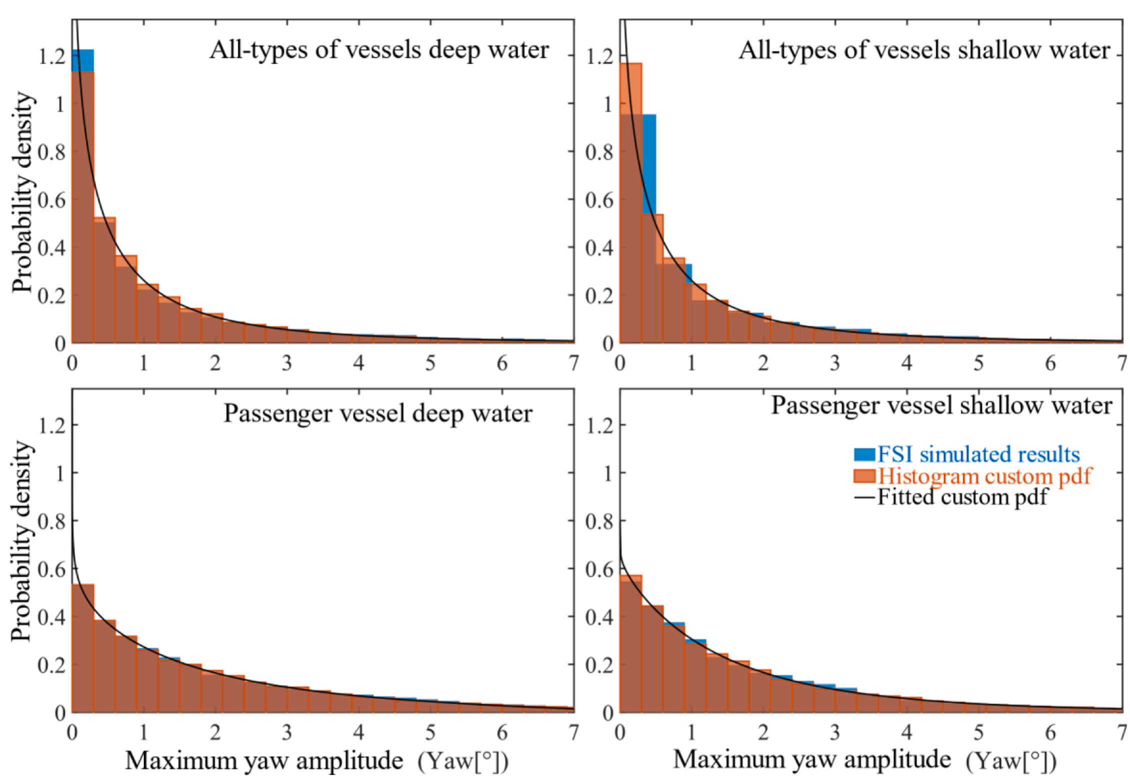

.

d) Fitted Burr type XII distributions of maximum yaw motion during a grounding event. Histograms display numerically simulated grounding ship motions and fitted pdfs. Input conditions account for deep and shallow waters for *passenger vessels* and *all-types of vessels*.

References

[1] Allianz Global. Safety and shipping review 2020. An annual review of trends and developments in shipping losses and safety. 2020.
[2] Zhang S, Pedersen PT, Villavicencio R. Probability of ship collision and grounding. Probab Mech Sh Collis grounding 2019:1–61. https://doi.org/10.1016/b978-0-12-815022-1.00001-3.
[3] HELCOM – Helsinki Commission. Ship accidents in the Baltic Sea during the period 1989 to 2018. Retrived from 2021. https://metadata.helcom.fi/geonetwork/srv/eng/catalog.search#/metadata/cae61cf8-0b3a-449a-aeaf-1df752dd3d80 (accessed November 5, 2021).
[4] Transportation safety board of Canada. Marine transportation safety investigation report M18C0225 (released 21 May 2021). 2021.
[5] SIAF. Safety Investigation Authority Finland. M2020-02 Grounding of M/S Amorella in the Åland archipelago on September 2020 (released 07 Sep 2021) in Finnish. 2020.
[6] SIAF. Safety Investigation Authority Finland. M2020-E2 M/S Viking Gracen karilleajo Maarianhaminassa 21.11.2020 (released 22 Dec 2020) in Finnish. 2020.
[7] Farley TJ, Paulsrud F. Norwegian/US coast guard. Report of investigation into the circumstances surrounding the grounding of the Monarch of The Seas on proselyte reef in Great Bay, Philipsburg, St Maarten, Netherlands Antilles on December 15 1998, resulting in major Vessel Dama. 2003.
[8] Papanikolaou A, Spanos D, Boulougouris E, Eliopoulou E, Alissafaki A. Investigation into the sinking of the RO-RO passenger ferry Express Samina. Int Shipbuild Prog 2004;51:95–120.
[9] Schröder-Hinrichs JU, Hollnagel E, Baldauf M. From Titanic to Costa Concordia—a century of lessons not learned. WMU J Marit Aff 2012;11:151–67.
[10] Abubakar A, Dow RS. Simulation of ship grounding damage using the finite element method. Int J Solids Struct 2013;50:623–36. https://doi.org/10.1016/j.ijsolstr.2012.10.016.
[11] Zhang S, Pedersen PT, Villavicencio R. Internal mechanics of ship collision and grounding. Probab Mech Sh Collis grounding 2019:147–270. https://doi.org/10.1016/b978-0-12-815022-1.00003-7.
[12] Cerup-Simonsen B, Törnqvist R, Lützen M. A simplified grounding damage prediction method and its application in modern damage stability requirements. Mar Struct 2009;22. https://doi.org/10.1016/j.marstruc.2008.06.007.
[13] Nguyen TH, Amdahl J, Garrè L, Leira BJ. A study on dynamic grounding of ships. Adv Mar Struct - Proc 3rd Int Conf Mar Struct MARSTRUCT 2011;2011:373–80. https://doi.org/10.1201/b10771-46.
[14] Brubak L, Hu Z, Kõrgesaar M, Schipperen I, Tabri K. Numerical simulations of grounding scenarios – benchmark study on key parameters in FEM moddling. Lect Notes Civ Eng 2021:257–69. https://doi.org/10.1007/978-981-15-4672-3_16.
[15] Heinvee M, Tabri K. A simplified method to predict grounding damage of double bottom tankers. Mar Struct 2015;43:22–43. https://doi.org/10.1016/j.marstruc.2015.04.002.
[16] Yu Z, Amdahl J. Full six degrees of freedom coupled dynamic simulation of ship collision and grounding accidents. Mar Struct 2016;47:1–22.
[17] Simonsen BC. Mechanics of ship grounding. Department of Naval Architecture and Offshore Engineering. Technical University of Denmark (DTU); 1997. PhD thesis.
[18] Hong L, Amdahl J. Plastic mechanism analysis of the resistance of ship longitudinal girders in grounding and collision. Ships Offshore Struct 2008;3:159–71. https://doi.org/10.1080/17445300802263849.
[19] Hong L, Amdahl J. Rapid assessment of ship grounding over large contact surfaces. Ships Offshore Struct 2012;7:5–19. https://doi.org/10.1080/17445302.2011.579003.
[20] Zeng J, Hu Z, Chen G. A steady-state plate tearing model for ship grounding over a cone-shaped rock. Ships Offshore Struct 2016;11:245–57. https://doi.org/10.1080/17445302.2014.985429.
[21] Sun B, Hu Z, Wang J. Bottom structural response prediction for ship-powered grounding over rock-type seabed obstructions. Mar Struct 2017;54:127–43. https://doi.org/10.1016/j.marstruc.2017.04.002.
[22] Friis-Hansen P, Ditlevsen O. Nature preservation acceptance model applied to tanker oil spill simulations. Struct Saf 2003;25. https://doi.org/10.1016/S0167-4730(02)00037-1.
[23] Lee SG, Lee JS, Lee HS, Park JH, Jung TY. Full-scale ship collision, grounding and sinking simulation using highly advanced M&S system of FSI analysis technique. Procedia Eng., vol. 173, Elsevier Ltd; 2017, p. 1507–14. Doi: 10.1016/j.proeng.2016.12.232.
[24] Lee SG, Zhao T, Nam JH. Structural safety assessment of ship collision and grounding using FSI analysis technique. Collis. Grounding Ships Offshore Struct. - Proc. 6th Int. Conf. Collis. Grounding Ships Offshore Struct. ICCGS 2013, Taylor and Francis - Balkema; 2013, p. 197–204. Doi: 10.1201/b14915-24.
[25] Kim SJ, Kõrgersaar M, Ahmadi N, Taimuri G, Kujala P, Hirdaris S. The influence of fluid structure interaction modelling on the dynamic response of ships subject to collision and grounding. Mar Struct 2021;75:102875. https://doi.org/10.1016/j.marstruc.2020.102875.
[26] Kim SJ, Kõrgersaar M, Taimuri G, Kujala P, Hirdaris S. A quasi-dynamic approach for the evaluation of structural response in ship collisions and groundings. Proc. Int. Offshore Polar Eng. Conf., vol. 2020- Octob, International Society of Offshore and Polar Engineers; 2020, p. 3174–80.
[27] Kim SJ, Taimuri G, Kujala P, Conti F, Le Sourne H, Pineau JP, et al. Comparison of numerical approaches for structural response analysis of passenger ships in collisions and groundings. Mar Struct 2022;81:103125. https://doi.org/10.1016/j.marstruc.2021.103125.
[28] Taimuri G, Kim SJ, Mikkola T, Hirdaris S. A two-way coupled FSI model for the rapid evaluation of accidental loads following ship hard grounding. J Fluids Struct 2022;112:103589. https://doi.org/https://doi.org/10.1016/j.jfluidstructs.2022.103589.
[29] Mazaheri A, Montewka J, Kujala P. Modeling the risk of ship grounding—a literature review from a risk management perspective. WMU J Marit Aff 2014;13:269–97. https://doi.org/10.1007/s13437-013-0056-3.
[30] Ringsberg JW. Characteristics of material, ship side structure response and ship survivability in ship collisions. Ships Offshore Struct 2010;5:51–66. https://doi.org/10.1080/17445300903088707.
[31] Liu Y, Frangopol DM. Probabilistic risk, sustainability, and utility associated with ship grounding hazard. Ocean Eng 2018;154. https://doi.org/10.1016/j.oceaneng.2018.01.101.
[32] Bulian G, Cardinale M, Dafermos G, Lindroth D, Ruponen P, Zaraphonitis G. Probabilistic assessment of damaged survivability of passenger ships in case of grounding or contact. Ocean Eng 2020;218:107396. https://doi.org/10.1016/j.oceaneng.2020.107396.
[33] Lützen M. Damage Distributions . EU-Project GRD1-1999-10721 "HARDER", Rep 2-22-D-2001-01-3 2001.
[34] Papanikolaou A, Hamann R, Lee BS, Mains C, Olufsen O, Vassalos D, et al. GOALDS - Goal Based Damage Ship Stability and safety standards. Accid Anal Prev 2013;60:353–65. https://doi.org/10.1016/j.aap.2013.04.006.
[35] Bulian G, Lindroth D, Ruponen P, Zaraphonitis G. Probabilistic assessment of damaged ship survivability in case of grounding: Development and testing of a direct non-zonal approach. Ocean Eng 2016;120:331–8. https://doi.org/10.1016/j.oceaneng.2016.02.018.
[36] Zaraphonitis G, Bulian G, Lindroth D, Hamann R, Luhmann H, Cardinale M, et al. Evaluation of risk from raking damages due to grounding, Final report. DNVGL Rep; 2015.
[37] Mauro F, Vassalos D. The influence of damage breach sampling process on the direct assessment of ship survivability. Ocean Eng 2022;250:111008. https://doi.org/10.1016/J.OCEANENG.2022.111008.
[38] Zhang M, Conti F, Le Sourne H, Vassalos D, Kujala P, Lindroth D, et al. A method for the direct assessment of ship collision damage and flooding risk in real conditions. Ocean Eng 2021;237:109605. https://doi.org/10.1016/j.oceaneng.2021.109605.
[39] Le Sourne H, Besnard N, Cheylan C, Buannic N. A ship collision analysis program based on upper bound solutions and coupled with a large rotational ship movement analysis tool. J Appl Math 2012;2012:375686. https://doi.org/10.1155/2012/375686.
[40] Mazaheri A, Ylitalo J. Comments on geometrical modeling of ship grounding. 5th Int. Conf Collis Grounding Ships 2010:235–43.
[41] Kehren FI, Krüger S. Development of a probabilistic methodology for damage stability regarding bottom damages. 10th Int. Symp. Pract. Des. Ships other Float. Struct. PRADS 2007, vol. 1, 2007, p. 174–81.
[42] Dong Y, Frangopol DM. Probabilistic ship collision risk and sustainability assessment considering risk attitudes. Struct Saf 2015;53. https://doi.org/10.1016/j.strusafe.2014.10.004.
[43] Youssef SAM, Paik JK. Hazard identification and scenario selection of ship grounding accidents. Ocean Eng 2018;153:242–55. https://doi.org/10.1016/j.oceaneng.2018.01.110.
[44] Taimuri G, Matusiak J, Mikkola T, Kujala P, Hirdaris S. A 6-DoF maneuvering model for the rapid estimation of hydrodynamic actions in deep and shallow waters. Ocean Eng 2020;218:108103. https://doi.org/10.1016/j.oceaneng.2020.108103.
[45] Taimuri G, Mikkola T, Matusiak J, Kujala P, Hirdaris S. The influence of hydrodynamic assumptions on ship maneuvering. 22nd Numer. Towing Tank Symp. (NuTTS 2019)-Tomar, Port., 2019, p. 6.
[46] NAPA. NAPA for Design Manuals; 2020.
[47] Luhmann H. Integrated flooding and standard for stability and crises management. FLOODSTAND deliverable No. D1.1b. Report FP7-RTD-218532; 2009.
[48] Friis-Hansen P, Simonsen BC. GRACAT: Software for grounding and collision risk analysis. Mar Struct 2002;15. Doi: 10.1016/S0951-8339(02)00009-6.
[49] Holtrop J, Mennen GGJ. An approximate power prediction method. Int Shipbuild Prog 1982;29:166–70.
[50] Söding H. Prediction of ship steering capabilities. Schiffstechnik 1982;29:3–29.
[51] Brix JE. Manoeuvring technical manual. Germany: Hamburg; 1993.
[52] Matusiak JE. Dynamics of a Rigid Ship - with applications. Aalto University 2021. http://urn.fi/URN:ISBN:978-952-64-0399-1;.
[53] Blendermann W. Parameter identification of wind loads on ships. J Wind Eng Ind Aerodyn 1994;51:339–51.
[54] Sakamoto T, Baba E. Minimization of resistance of slowly moving full hull forms in short waves. Proc Sixt Symp Nav Hydrodyn 1986:598–613.

[55] Faltinsen OM. Sea loads on ships and offshore structures; 1990.
[56] Faltinsen OM, Minsaas KJ, Liapis N, Skjordal SO. Prediction of resistance and propulsion of a ship in a seaway. Proc 13th Symp Nav Hydrodyn Tokyo 1980:1–19.
[57] Raven HC. A new correction procedure for shallow-water effects in ship speed trials. PRADS 2016 - Proc. 13th Int. Symp. Pract. Des. Ships Other Float. Struct.; 2016.
[58] Ankudinov VK, Miller ER, Jakobsen BK, Daggett LL. Manoeuvring performance of tug/barge assemblies in restricted waterways. Proc MARSIM ICMS 1990:515–25.
[59] Kijima K, Nakiri Y, Tsutsui Y, Matsunaga M. Prediction method of ship manoeuvrability in deep and shallow waters. Int. Conf. Mar. Simul. Sh. Maneuverability (MARSIM '90); 1990, p. 311.
[60] Badouel D. An efficient ray - polygon intersection. Graph Gems, Elsevier Inc 1990: 390–3. https://doi.org/10.1016/B978-0-08-050753-8.50082-6.
[61] Moller T, Trumbore B. Fast, minimum storage ray-triangle intersection. Chalmers Tekniska Hogskola; 1998. Doi: 10.1201/b10628-23.
[62] IMO. SOLAS consolidated text of the International Convention for the safety of life at sea, 1974, and its protocol of 1988 : articles, annexes and certificates : incorporating all amendments in effect from 1 January 2020. International Maritime Organization; 2020; 2020.
[63] Ruponen P, Manderbacka T, Lindroth D. On the calculation of the righting lever curve for a damaged ship. Ocean Eng 2018;149. https://doi.org/10.1016/j.oceaneng.2017.12.036.
[64] Ruponen P, Lindroth D, Routi AL, Aartovaara M. Simulation-based analysis method for damage survivability of passenger ships. Sh Technol Res 2019;66. https://doi.org/10.1080/09377255.2019.1598629.
[65] Matsumoto M, Nishimura T. Mersenne Twister: A 623-Dimensionally Equidistributed Uniform Pseudo-Random Number Generator. ACM Trans. Model. Comput. Simul., vol. 8, 1998. https://doi.org/10.1145/272991.272995.
[66] MATLAB. Matlab 2021. MathWorks, Inc; 2021:1.
[67] NAPA. NAPA for Design Manuals 2021.2. 2021.